Scientific report; WR 96-01

KNMI

A new algorithm for total ozone retrieval from direct sun measurements with a filter instrument

W.M.F. Wauben

De Bilt, 1996

Scientific report= wetenschappelijk rapport; WR 96-01

De Bilt, 1996

Postbus 201
3730 AE De Bilt
Wilhelminalaan 10
Telefoon 030-220 69 11
telefax 030-221 04 07

Auteurs: W.M.F. Wauben

UDC: 551.501.71
551.501.721
551.510.534
551.508.952

ISSN: 0169-1651

ISBN: 90-369-2105-8

A new algorithm for total ozone retrieval from direct sun measurements with a filter instrument

W.M.F. Wauben

KNMI, P.O.Box 201, 3730 AE De Bilt, The Netherlands

March 19, 1996

Contents

Abstract

In this report a new algorithm is presented which derives the ozone column density from attenuated direct solar radiation measured at two wavelengths in the ultraviolet. The attenuation of direct solar radiation by ozone, molecules and aerosol is considered in this retrieval algorithm for so-called total ozone. A correction is applied for the spectral attenuation by molecular scattering and the attenuation by aerosol is assumed to be independent of wavelength. The ozone column density can then be derived by using the spectral dependence of the ozone absorption cross-section in combination with the spectrum of the incident solar radiation. If the measurements are absolutely calibrated, the aerosol optical thickness can also be obtained.

The so-called direct sun observations described above can be performed with a filter instrument that measures in two selected wavelength bands in the ultraviolet. The spectral dependence of the incident solar radiation, molecular scattering and absorption by ozone are considered explicitly in the retrieval algorithm as well as the spectral sensitivity of the filter instrument, which results from both the spectral dependence of the filter transmission and the sensitivity of the detector. The effect of this so-called filter function of the instrument on the observed direct solar radiation is important at short wavelengths and when the bandwidth of the instrument is large. The correction of the derived ozone column density for this so-called bandwidth effect generally depends on both the solar elevation and the ozone column density itself.

The algorithm is tested with simulated direct sun radiances calculated with an atmospheric shell model. The sensitivity of the retrieved ozone column density to various assumptions and uncertainties in the algorithm is also investigated. It is found that the accuracy of the derived ozone column density is mainly affected by: (i) the wavelength dependence of aerosol leading to an overestimation of the ozone column density; (ii) errors in the filter function of the instrument; and (iii) the presence of diffuse radiation resulting in an underestimation of the ozone column density, especially for low solar elevations. These errors can partly be avoided by performing measurements under favourable conditions such as clear atmospheres, high solar elevations and by careful determination of the filter function of the instrument.

Chapter 1

Introduction

Ozone is an important trace gas in the Earth's atmosphere (IPCC 1995, CEC 1993 and WMO 1994). It is a reactive gas that plays a key role in atmospheric chemistry. Ozone has strong absorption bands in the infrared, and therefore it influences the energy budget of the Earth's atmosphere. In addition, ozone has a strong absorption band in the ultraviolet and a weaker band in the visible. It protects the biosphere by absorbing almost all harmful solar ultraviolet radiation. However, high levels of ozone near the Earth's surface leads to health problems and damage to vegetation. Only about 10% of the ozone column density can be found in the troposphere, i.e. the lower part of the atmosphere where the temperature generally decreases with altitude. The troposphere extends up to about 10 km at midlatitudes and contains about 90% of the mass of the atmosphere. The stratosphere, which is a layer between about 10 to 50 km, contains about 90% of the ozone. In the stratosphere the temperature increases with altitude mainly because of the heat generated by the absorption of ultraviolet radiation by ozone. The tropopause is the boundary between the troposphere and stratosphere. Therefore, a low elevation of the tropopause, i.e. a high pressure at the tropopause, generally corresponds with large ozone column density.

Ozone is continuously being created and destroyed by chemical processes under the influence of ultraviolet radiation. However, because the chemical lifetime of ozone is in the order of months, rapid variations in the ozone column density are mainly the result of transport. The elevation of the tropopause varies with meteorological systems, and therefore the ozone column density can also undergo large day-to-day variations. Figure 1.1 shows the daily mean ozone column densities measured with a Brewer spectrophotometer at De Bilt in 1994 together with the corresponding heights of the tropopause derived from temperature profiles measured with radiosondes. The ozone column density shows large day-to-day variations which are up to some degree correlated with the variations in the height of the tropopause. The correlation coefficient of the curves is 0.62. Generally, a high pressure system at the surface corresponds with a high elevation of the tropopause. Therefore the surface pressure will be anti-correlated with the ozone column density. The surface pressure measured at de Bilt in 1994 is also presented in Fig. 1.1. As could be expected, the correlation between surface pressure and ozone column density, which is only -0.27, is less than

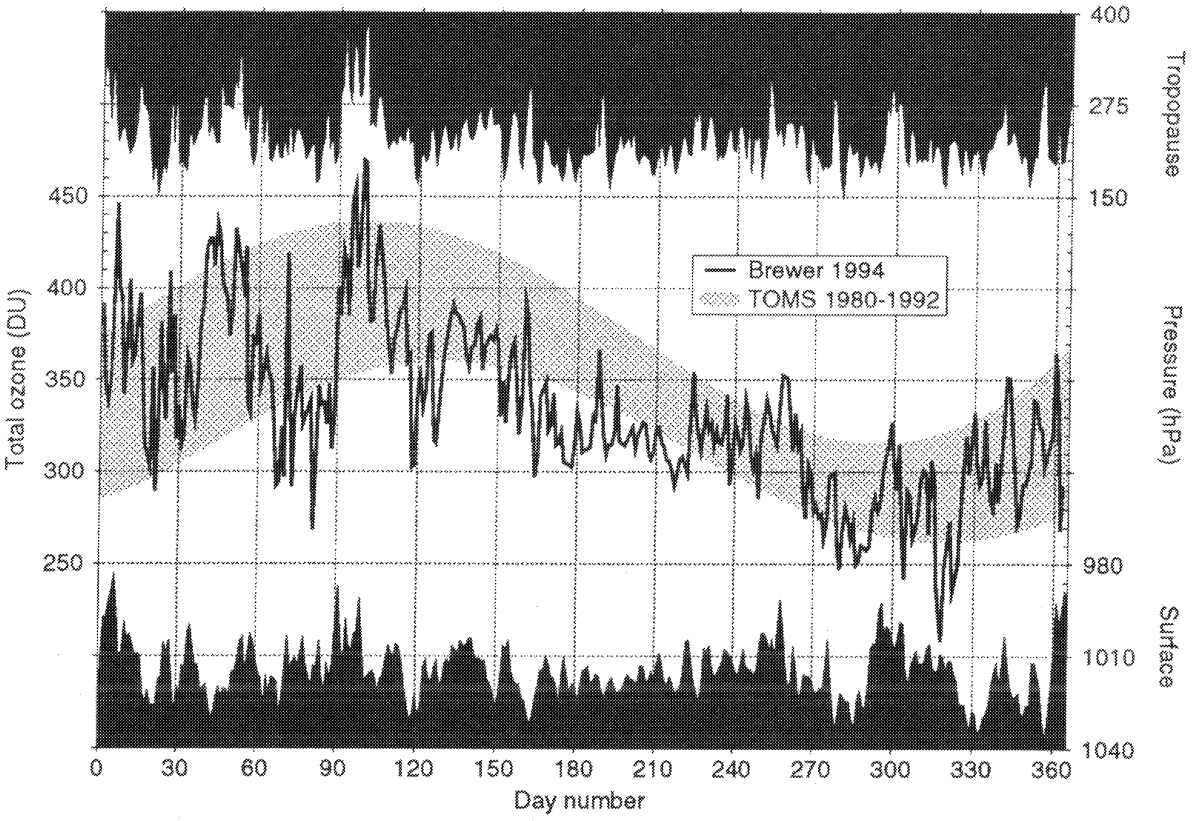

Figure 1.1 Daily mean total ozone in Dobson Units for De Bilt in 1994 measured with the Brewer spectrophotometer together with the corresponding pressure at the tropopause derived from radiosonde temperature profiles and the surface pressure in hPa. The range of the long-term total ozone for De Bilt according to TOMS satellite data over the period 1980-1992 is also given.

the correlation between the pressure at the tropopause and total ozone. In addition, the ozone column density depends on many other meteorological parameters (cf. Fortuin & Kelder 1996). For example, the correlation between surface temperature and total ozone is -0.31 for the measurements at De Bilt over 1994. During spring and summer this correlation is -0.64. The long-term mean ozone column density obtained by averaging 12 years of TOMS satellite ozone observations for the pixel containing De Bilt is also given in Fig. 1.1. Here the shaded region indicates the mean ± 1 standard deviation of the long-term ozone data. This long-term mean shows the seasonal variation of the ozone column density with a maximum in spring and a minimum in autumn. This seasonality is due to the variations in stratospheric transport of ozone rich air from the tropics towards the polar region of the winter hemisphere. The figure also shows that the actual ozone column densities may deviate considerably from the long-term mean values.

Because ozone plays an important role in both the atmosphere and biosphere it is important to monitor the ozone column density. Especially, since the amount

of ozone in the atmosphere has been influenced by anthropogenic activities (WMO 1994). Emissions of CFC's caused ozone depletion in the stratosphere (cf. Farman *et al.* 1985), whereas emissions of nitrogen oxides and methane lead to an increase of tropospheric ozone (cf. Crutzen & Zimmermann 1991). Furthermore, natural processes such as the Mount Pinatubo eruption affected the ozone layer (cf. e.g. Kinnison *et al.* 1994). The ozone column density is monitored using both satellite and surface observations. The surface observations are mainly performed by Dobson and Brewer spectrophotometers. The Dobson spectrophotometer is the standard instrument to measure the ozone column density (cf. Dobson 1957). It is a relatively cumbersome quartz prism double monochromator which is operated manually and is not weatherproof. The Brewer spectrophotometer (Kerr *et al.* 1985) uses a grating to select the wavelength band that is incident on the photomultiplier. This instrument is fully automated and weatherproof. Therefore, the Brewers are gradually taking over from the Dobsons. However, both instruments are delicate and expensive, but when calibrated, operated and maintained carefully, they give accurate ozone column densities with an error of about 1%. The use of optical filters to select the ultraviolet bands is appealing because it allows the construction of small, ragged and relatively inexpensive spectrophotometers. Several filter instruments have been considered. The instruments using glass absorption filters, such as the Russian M-83 spectrophotometers (cf. WMO 1988), produced inaccurate ozone columns with errors of about 40 % because of the broad transmittance bands of the glass absorption filters (Bojkov 1969). Interference filter ozone spectrophotometers, such as the New Zealand Mark instruments (cf. Matthews *et al.* 1974), contain more suitable narrow band filters. These filters still cause problems which are mainly the result of uncertainties in center wavelength due to calibration and aging and the presence of leakage bands (cf. Basher & Matthews 1977). Furthermore, the spectral characteristics of the interference filters are temperature dependent. The overall accuracy of the ozone column densities derived from interference filter spectrophotometers is about 5%.

In this paper an interference filter instrument is considered that measures the attenuated direct solar radiation at 2 wavelengths bands in the ultraviolet. The ratio of these two measurements can be used to derive the ozone column density. This instrument is being developed by KNMI and Kipp & Zonen for educational purposes. Unlike the TOPS instrument (cf. Mims 1992) our instrument uses only one interference filter to perform the measurements at two wavelengths bands, since tilting such a filter with respect to the photodiode results in a small, but sufficient, wavelength shift of the spectral sensitivity of the filter. This handy and relatively inexpensive filter instrument will be able to produce relatively accurate ozone column densities under clear sky conditions, i.e. an accuracy of about 10% is envisaged. In addition, the instrument can yield calibrated narrow band irradiances and could therefore also be used for monitoring UV and aerosol optical thicknesses. A retrieval algorithm is presented in this paper that can be used to derive the ozone column density from

direct sun measurements in two relatively broad wavelengths bands in the ultraviolet. As a result of the spectral sensitivity of the filter the measurements yield wavelength-weighted irradiances. This bandwidth effect of the filter is explicitly taken into account in the algorithm and is not treated by means of bandwidth equivalent coefficients together with precalculated correction terms (cf. e.g. Basher 1977). The algorithm is tested with simulated direct sun irradiances calculated with an atmospheric model. The sensitivity of the retrieved ozone column density to the various assumptions and uncertainties in the algorithm is also investigated.

Chapter 2

Attenuation of radiation

Solar irradiance, S_λ (in $\mathrm{Wm^{-2}nm^{-1}}$) where λ denotes the wavelength (in nm), is unidirectionally incident at the top of the Earth's atmosphere. This irradiance is the energy flux per unit wavelength through a plane of unit area perpendicular to the direction of the incident solar radiation. Here UVB radiation, i.e. ultraviolet radiation between 290 and 330 nm, is considered. When this radiation traverses through a cloudless atmosphere it is attenuated by absorption and scattering by molecules and suspended particles, also called aerosol. The amount of radiation I_λ attenuated per optical path length ℓ_λ is proportional to the radiation itself, i.e. $dI_\lambda/d\ell_\lambda = I_\lambda$. The radiation which after one or more scattering events contributes to the radiation on the right hand side of this expression, i.e. the so-called diffuse radiation, is neglected. The solution of the above expression shows that the attenuated radiation is proportional to $\exp(-\ell_\lambda)$. Therefore, the amount of direct, i.e. unscattered, radiation, D_λ, that reaches the surface is then related to the radiation incident at the top of the atmosphere according to the Lambert-Beer-Bouguer law (cf. e.g. Iqbal 1983)

$$D_\lambda = S_\lambda \exp(-b_\lambda m_r), \tag{2.1}$$

where m_r is the relative airmass factor which converts the dimensionless vertical optical thickness b_λ into the slant optical path length of the radiation ℓ_λ. If the curvature of the Earth's atmosphere and refraction are neglected, the relative airmass factor is given by

$$m_r = \frac{1}{\sin\gamma}, \tag{2.2}$$

with γ the solar elevation (in degrees). The sphericity of and refraction in the atmosphere must be taken into account when applying the retrieval algorithm to actual measurements (cf. Sec. 4.8). Because of the different vertical distribution of these attenuating substances three different relative airmass factors for absorption by ozone, scattering by molecules and absorption and scattering by aerosol are required These three relative airmass factors are denoted by m_{r,O_3}, $m_{r,mol}$ and $m_{r,aer}$, respectively.

Attenuation of UVB radiation in a cloudless Earth's atmosphere occurs mainly through absorption by ozone. The absorption optical thickness of ozone, b_{λ,O_3}, equals

the product of the ozone column density, d_{O_3} (in cm^{-2}), and the absorption cross-section per ozone molecule, σ_{λ,O_3} (in cm^2), i.e.

$$b_{\lambda,O_3} = d_{O_3}\sigma_{\lambda,O_3}. \tag{2.3}$$

The ozone column density can also be expressed in the more commonly used Dobson units (DU) by using

$$2.68675 \times 10^{16} \text{ ozone molecules/cm}^2 = 1 \text{ DU}. \tag{2.4}$$

A Dobson unit expresses the ozone column density as the thickness (in 0.01 mm) of a layer under standard conditions at the Earth's surface containing the same amount of ozone. The spectral dependence of the ozone absorption cross-section is given in Fig. 4.1 for different temperatures. In this study the ozone absorption cross-section at 228 K is adopted for the retrieval algorithm. The influence of the temperature dependence of the ozone absorption cross-section will be investigated in Sec. 4.3.

Scattering by molecules also contributes significantly to the attenuation of solar UVB radiation in the Earth's atmosphere. The approximate expression for the molecular optical thickness

$$b_{\lambda,mol} = \frac{P}{1013.25} 8.569 \times 10^9 \lambda^{-4} \left(1 + 1.13 \times 10^4 \lambda^{-2} + 1.3 \times 10^8 \lambda^{-4}\right) \tag{2.5}$$

of Hansen & Travis (1974) is used in the present study, where P denotes the surface pressure (in hPa) and λ the wavelength (in nm). Other expressions for the molecular optical thickness are considered in Sec. 4.2 in order to study the effect of its uncertainty. Unlike absorbed radiation, scattered radiation can contribute to the radiation in the direction of the direct solar radiation. In Sec. 4.7 the effect this diffuse radiation is investigated.

The characteristics of scattering and absorption by aerosol are largely unknown. However, its contribution to the attenuation of solar UVB radiation is smaller than that of absorption by ozone and scattering by molecules for clear atmospheres. The spectral dependence of the optical properties of aerosol is not large, so that the aerosol optical thickness, b_{aer}, is assumed to be independent of wavelength. This assumption is investigated in Sec. 4.4 by considering different expressions for the wavelength dependence of the aerosol optical properties that are found in the literature.

The attenuation of radiation resulting from absorption by ozone, scattering by molecules, and scattering and absorption by aerosol is given by

$$b_\lambda = b_{\lambda,O_3} + b_{\lambda,mol} + b_{aer}. \tag{2.6}$$

The direct solar radiation reaching the surface, Eq. (2.1), can then be written as

$$D_\lambda = S_\lambda \exp(-d_{O_3}\sigma_{\lambda,O_3} m_{r,O_3} - b_{\lambda,mol} m_{r,mol} - b_{aer} m_{r,aer}), \tag{2.7}$$

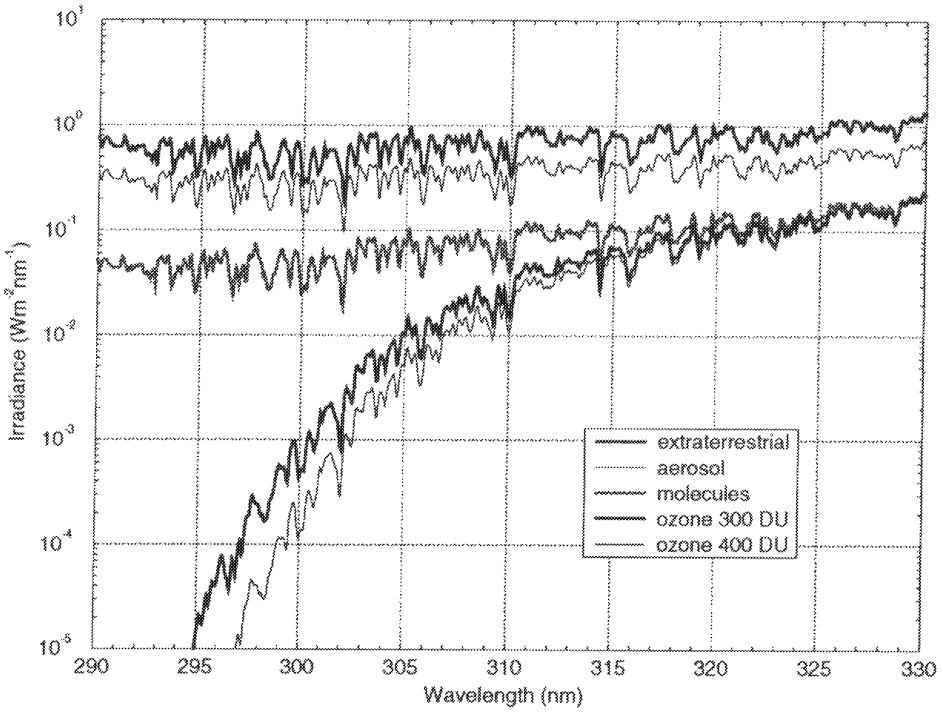

Figure 2.1 Illustration of the spectral solar irradiance incident at the top of the atmosphere and the radiation reaching the surface. The attenuation resulting from aerosol, molecules and ozone is shown for a model atmosphere with a solar elevation of 45°. Ozone column densities of 300 and 400 DU are considered.

where $b_{\lambda,mol}$ is given by Eq. (2.5) and m_r by Eq (2.2). Note that for actual measurements the relative airmass factor given in Eq. (4.20) is used, with typical heights of 22, 5 and 1 km for attenuation by ozone, molecules and aerosol, respectively.

Figure 2.1 shows the spectral dependence of the solar radiation incident at the top of the atmosphere and the attenuated direct solar radiation reaching the surface. The so-called SUSIM spectrum is used for the solar extraterrestrial irradiance (cf. Sec. 4.6). The attenuation of direct solar radiation is evaluated according to Eq. (2.7) by using Ångström's turbidity coefficient for the aerosol optical thickness with $\alpha = 1.3$ and $\beta = 0.1$ (cf. Sec. 4.4); the molecular optical thickness of Hansen & Travis (1974) with a surface pressure of 1013 hPa (cf. Eq. (2.5)) and the ozone absorption cross-sections of Bass & Paur (1985) at -45°C (cf. Sec. 4.3) and ozone column densities of 300 and 400 DU. Figure 2.1 shows that the extraterrestrial solar irradiance varies increases only slightly from 290 to 330 nm. However, it has many spectral features due to absorption in the outer layers of the solar atmosphere. The attenuation by aerosol is almost independent of wavelength and the attenuation by molecules differs almost a factor of 2 between 290 and 330 nm. Ozone attenuation is negligible for wavelengths larger than 325 nm but it increases rapidly with decreasing wavelength. Below about 305 nm absorption by ozone is the dominant attenuation process. The spectral dependence of the UVB irradiance reaching the surface is very sensitive to the ozone column density due to the strong wavelength dependence of the ozone absorption. Therefore, the

ozone column density can de derived from direct sun measurements at 2 different wavelengths in the UVB.

Chapter 3

Retrieval algorithm

The direct solar radiation reaching the surface is, according to Eq. (2.7), given by

$$D_\lambda = S_\lambda \exp(-d_{O_3}\sigma_{\lambda,O_3}m_{r,O_3} - b_{\lambda,mol}m_{r,mol} - b_{aer}m_{r,aer}), \tag{3.1}$$

with S_λ the solar radiation incident at the top of the atmosphere with wavelength λ, d_{O_3} the ozone column density, σ_{λ,O_3} the ozone absorption cross-section, $b_{\lambda,mol}$ the molecular optical thickness, b_{aer} the aerosol optical thickness and m_r the relative airmass factor for each of the three components individually. Of the variables on the right hand side of Eq. (3.1) only the ozone column density and the aerosol optical thickness are unknown. All the other variables involved in the expression as well as their spectral dependence are known. Their values are given in Chapters 2 and 4. Therefore, two measurements of the direct solar radiation at different wavelengths can be combined to eliminate the wavelength independent aerosol optical thickness. Division of Eq. (3.1) for λ_1 by the corresponding expression for λ_2 gives after rearranging terms and taking the natural logarithm

$$\log\left(\frac{D_{\lambda_1}}{S_{\lambda_1}}\right) - \log\left(\frac{D_{\lambda_2}}{S_{\lambda_2}}\right) = d_{O_3}(\sigma_{\lambda_2,O_3} - \sigma_{\lambda_1,O_3})m_{r,O_3} + (b_{\lambda_2,mol} - b_{\lambda_1,mol})m_{r,mol}. \tag{3.2}$$

From this equation the ozone column density can be derived. Since this method uses the ratio of 2 measurements the absolute calibration of the instrument is not needed, but only the ratio of the sensitivity of the instrument at the 2 wavelengths. The absolute value of the incident solar radiation, which is a function of the day of the year because of variations in the distance between Sun and Earth, is therefore also not required. An absolute calibration is however needed if one wants to obtain the aerosol optical thickness from Eq. (3.1) once the ozone column density has been derived.

The measurement is complicated by the fact that it is not performed monochromatically. A so-called filter function, F_λ, gives the sensitivity of the instrument as a function of wavelength (cf. Fig. 4.2). Therefore, a measurement of the direct solar radiation yields a wavelength weighted value given by

$$< D_\lambda >= \frac{1}{N}\int_0^\infty F_\lambda D_\lambda d\lambda, \tag{3.3}$$

where the brackets denote the wavelength weighted value of a variable and N is the normalization of the filter

$$N = \int_0^\infty F_\lambda d\lambda. \tag{3.4}$$

Hence, the measurement is performed in a wavelength band determined by the filter function which is characterized by the central wavelength

$$\lambda_c = \frac{1}{N} \int_0^\infty F_\lambda \lambda d\lambda, \tag{3.5}$$

the width of the filter function

$$w = \frac{N}{F_{max}}, \tag{3.6}$$

and the maximum sensitivity of the filter function F_{max}. Note that in general, the filter functions for the two wavelengths under consideration are different. The wavelength weighted value $< D_\lambda >$ should be equal to the wavelength weighted value of the expression on the right-hand side of Eq. (3.1). However, the wavelength weighted value of a product of factors generally differs from the product of wavelength weighted values of the individual factors, i.e. $< a_\lambda b_\lambda > \neq < a_\lambda >< b_\lambda >$. Therefore, the ozone column density cannot be derived from measurements at 2 wavelength bands by using Eq. (3.2) with wavelength weighted values for the individual terms occurring on the right hand side of this expression.

The effect of the filter function is illustrated with some numerical simulations. The expression on the right hand side of Eq. (3.1) is evaluated using: the SUSIM spectrum for the extraterrestrial solar radiation (cf. Sec. 4.6); the ozone absorption cross-section of Bass & Paur (1984) at -45°C (cf. Sec. 4.3); the molecular optical thickness of Hansen & Travis (1974) for a surface pressure of 1013 hPa (cf. Eq. (2.5)) and Ångström's turbidity coefficient for the aerosol optical thickness with $\alpha = 1.3$ and $\beta = 0.1$ (cf. Sec. 4.4). The expression on the right hand side of Eq. (3.1) is evaluated for each wavelength separately and afterwards integrated over wavelength, i.e. $< a_\lambda b_\lambda >$ is calculated, or the individual terms are first integrated over wavelength before the different terms are combined, i.e. $< a_\lambda >< b_\lambda >$ is calculated. A Gaussian filter function (cf. Sec. 4.5) with $F_{max} = 1$ is assumed. The two evaluations of the wavelength weighted right hand side of Eq. (3.1) are performed by using various solar elevations for the calculation of the relative airmass factors for the three constituents (cf. Eq. (4.20)), several ozone column densities, and different central wavelengths and widths of the filter function. Figure 3.1 shows a contour plot of the ratio $< a_\lambda >< b_\lambda > / < a_\lambda b_\lambda >$ as a function of central wavelength and width of the filter function using a ozone column density of 325 DU and a solar elevation of 45°. The results indicate that the effect of the filter function generally increases with decreasing central wavelength and with increasing width. The effect of the filter function is significant, i.e. gives deviations larger than 1%, for central wavelengths smaller than about 10 nm and widths larger than about 1 nm. The bandwidth effect is mainly the result of the

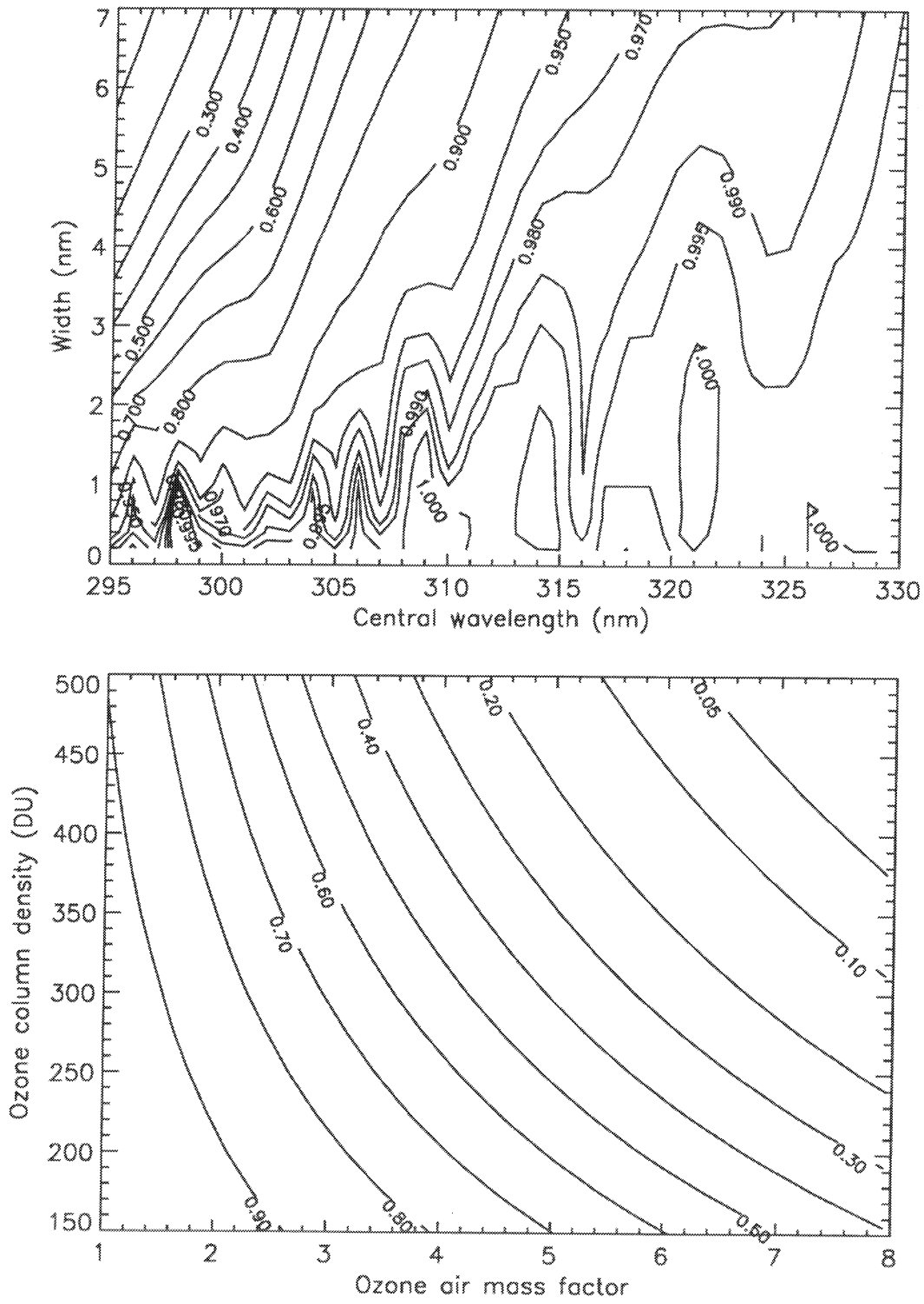

Figure 3.1 Contour plot of the ratio $< S_\lambda > \exp(-d_{O_3} < \sigma_{\lambda,O_3} - > m_{r,O_3} - < b_{\lambda,mol} > m_{r,mol} - < b_{aer} > m_{r,aer}) / < S_\lambda \exp(-d_{O_3}\sigma_{\lambda,O_3} m_{r,O_3} - b_{\lambda,mol} m_{r,mol} - b_{aer} m_{r,aer}) >$ as a function of the central wavelength and width of the filter function (top) and as a function of the relative airmass factor of ozone and the ozone column density (bottom). For more information see text.

strong spectral dependence of the ozone absorption cross-section. The dependence on the relative airmass factor of ozone and the ozone column density of the effect of the filter function on the ratio $< a_\lambda >< b_\lambda > / < a_\lambda b_\lambda >$ is given in the lower panel of Fig. 3.1 for a Gaussian filter function with central wavelength 306 nm and width 3.6 nm. Note that the ratio at e.g. $m_{r,O_3} = 6$ and $d_{\lambda,O_3} = 150$ DU differs from that at $m_{r,O_3} = 3$ and $d_{\lambda,O_3} = 300$ DU. Therefore, the effect of the filter function does not depend on the slant ozone column density $n_{\lambda,O_3} m_{r,O_3}$, but depends on the ozone column density and ozone airmass factor individually. Hence, no prescribed correction factor for the effect of the filter function as function of the slant ozone column density can be used.

The ozone column density cannot be derived by using Eq. (3.2), but instead Eq. (3.1) has to be solved iteratively. For this the filter function of the instrument has to be accurately known. The first step in the iteration procedure is using the approximation that the wavelength weighted value of a product of factors equals the product of the wavelength weighted values of the individual factors. A first estimate of the ozone column density can then be obtained form Eq. (3.2) according to

$$\log\left(\frac{N_1 < D_{\lambda_1} >}{N_1 < S_{\lambda_1} >}\right) - \log\left(\frac{N_2 < D_{\lambda_2} >}{N_2 < S_{\lambda_2} >}\right) = d^1_{O_3}(< \sigma_{\lambda_2,O_3} > - < \sigma_{\lambda_1,O_3} >) m_{r,O_3} + (< b_{\lambda_2,mol} > - < b_{\lambda_1,mol} >) m_{r,mol}, \quad (3.7)$$

where $N_1 < D_{\lambda_1} >$ and $N_2 < D_{\lambda_2} >$ are the measured values of the attenuated direct solar radiation; $N_1 < S_{\lambda_1} >$ and $N_2 < S_{\lambda_2} >$ are the wavelength weighted values of the incident solar radiation (cf. Sec. 4.6); $< \sigma_{\lambda_1,O_3} >$ and $< \sigma_{\lambda_2,O_3} >$ are the wavelength weighted values of the ozone absorption cross-section (cf. Sec. 4.3); $< b_{\lambda_1,mol} >$ and $< b_{\lambda_2,mol} >$ are the wavelength weighted values of the molecular optical thickness (cf. E. (2.5)); and m_{r,O_3} and $m_{r,mol}$ are the relative airmass factors given by Eq. (4.20). Hence, Eq. (3.7) can be solved for $d^1_{O_3}$, i.e. the first estimate of the ozone column density. The next steps of the iteration procedure correct the estimated value of $d^i_{O_3}$ obtained in the previous iteration step, starting from $d^1_{O_3}$, with a correction term $\Delta d^i_{O_3}$ leading to a better approximate solution $d^{i+1}_{O_3} = d^i_{O_3} + \Delta d^i_{O_3}$. Substitution of this next approximation $d^{i+1}_{O_3}$ for d_{O_3} in Eq. (3.1) gives

$$D_\lambda = Y_\lambda \exp(-\Delta d^i_{O_3} \sigma_{\lambda,O_3} m_{r,O_3}) \exp(-b_{aer} m_{r,aer}), \quad (3.8)$$

where

$$Y_\lambda = S_\lambda \exp(-d^i_{O_3} \sigma_{\lambda,O_3} m_{r,O_3} - b_{\lambda,mol} m_{r,mol}). \quad (3.9)$$

Assuming that $< Y_\lambda \exp(-\Delta d^i_{O_3} \sigma_{\lambda,O_3} m_{r,O_3}) >=< Y_\lambda >< \exp(-\Delta d^i_{O_3} \sigma_{\lambda,O_3} m_{r,O_3}) >$ because $\Delta d^i_{O_3}$ is small, enables computation of the wavelength weighted value of Y_λ since $d^i_{O_3}$ has been derived in the previous iteration step and all other parameters are known. The correction term for the ozone column density can then be obtained from

the measured ratio's by using

$$\log\left(\frac{N_1 < D_{\lambda_1} >}{N_1 < Y_{\lambda_1} >}\right) - \log\left(\frac{N_2 < D_{\lambda_2} >}{N_2 < Y_{\lambda_2} >}\right) = \Delta d^i_{O_3}(< \sigma_{\lambda_2,O_3} > - < \sigma_{\lambda_1,O_3} >) m_{r,O_3}. \tag{3.10}$$

This yields a new estimate for the ozone column density $d^{i+1}_{O_3} = d^i_{O_3} + \Delta d^i_{O_3}$. The iteration procedure given above can be repeated to get better estimates of the ozone column density, until the correction term is negligible.

An actual measurement yields $N < D_\lambda >$, where the factor N cancels the normalization of the filter which occurs in the wavelength weighting (cf. Eq. (3.3)). Thus $N < D_\lambda >$ takes the attenuation by the filter function into account. The aerosol optical thickness can be obtained from

$$\log\left(\frac{N < S_\lambda \exp(-d_{O_3}\sigma_{\lambda,O_3} m_{r,O_3} - b_{\lambda,mol} m_{r,mol}) >}{N < D_\lambda >}\right) = b_{aer} m_{r,aer} \tag{3.11}$$

once the ozone column density has been derived. The above equation can be applied to the measurements at both wavelength bands. However, the instrument that is used for measuring the direct solar radiation must be calibrated absolutely in order to allow derivation of the aerosol optical thickness. Furthermore, variations of up to about ± 3 % in the solar irradiance incident at the top of the atmosphere resulting from seasonal changes in the Sun-Earth distance have to be taken into account (cf. Sec. 4.6).

Chapter 4

Tests of the algorithm

In this section the algorithm presented in Chapter 3 is tested. Since actual measurements are not yet available, the algorithm is tested by using surface irradiances obtained with model calculations. In order to perform the model calculations certain assumptions about the structure of the atmosphere and the radiative processes occurring in it have to be made. In addition, the scattering and absorption properties of the atmospheric constituents in this atmospheric model are not accurately known. Therefore the model calculations may give surface irradiances that differ from observed irradiances. However, using model calculations to simulate the signal that an instrument measures has the advantage that the accuracy of the retrieval algorithm can be tested and the sensitivity of the results to various assumptions in the retrieval algorithm can be studied. Another advantage is that uncertainties related to the instrument that would be used for the actual measurements can be circumvented or investigated. Such tests and sensitivity studies of the ozone retrieval algorithm by using modelled surface irradiances are presented in the following sections.

The atmospheric model that is used for simulating the direct sun measurements takes scattering and absorption by trace gases, molecules and aerosol into account. Model calculations have been performed for the mid-latitude summer (MLS) and winter (MLW) standard atmospheres (Anderson *et al.* 1986). The pressure and temperature profiles of these atmospheres are used to calculate the molecular scattering cross-section at each altitude (cf. Sec. 4.2). Integration of the molecular scattering cross-section over altitude gives the wavelength dependent molecular optical thickness. The ozone profile together with the temperature profile and the temperature dependent ozone absorption cross-section of Bass & Paur (1984) and Paur & Bass (1984) gives the spectral ozone absorption optical thickness (cf. Sec. 4.3). An actual ozone column density of 334 DU is obtained for the MLS standard atmosphere and 378 DU for the MLW atmosphere. Absorption by sulpherdioxide and nitrogendioxide are also considered by using their profiles in combination with the absorption cross-section of Hearn & Joens (1991) and Schneider *et al.* (1987), respectively. The resulting column densities of sulpherdioxide and nitrogendioxide are 0.1 and 0.2 DU, respectively, for both atmospheres. The aerosol scattering and absorption properties as well as their variation with altitude are taken from the LOWTRAN 7 model (Kneizys *et al.* 1988).

For the model calculations presented here the rural aerosol at 80 % relative humidity and with 10 km visibility is considered in the boundary layer (0-2 km); tropospheric aerosol at 80 % relative humidity and with 23 km visibility is used between 2-10 km; background stratospheric aerosol is employed in the stratosphere (10-30 km); and meteoric aerosol is used in the upper atmosphere (30-100 km). In addition, empirical expressions for the spectral dependence of the aerosol optical thickness are considered. These expressions are used to test the assumption of an aerosol optical thickness independent of wavelength (cf. Sec. 4.4).

The SUSIM extraterrestrial solar spectrum (cf. Sec. 4.6) is assumed to be incident at the top of the atmosphere model. The attenuation of this radiation through scattering and absorption by the atmospheric constituents mentioned above is given by the Lambert-Beer-Bouguer law (cf. Eq. (2.1)). The amount of radiation received by the instrument is obtained by integration of the spectral surface irradiance over the 'actual' filter function centered at 306 nm (cf. Sec. 4.5). This represents the wavelength weighted value of the direct solar radiation reaching the surface that is observed by the instrument. For the second wavelength band of the instrument the same filter function is used, but centered either at 302 or 310 nm. The effect of diffuse, i.e. scattered, radiation is investigated in Sec. 4.7 with a radiative transfer model coupled to the optical parameters generated by the atmospheric model (cf. Stammes *et al.* 1996) and considering an isotropically reflecting surface with an albedo of 0.05. The so-called adding-doubling radiative transfer method (cf. e.g. De Haan *et al.* 1987) is employed to account for the full angular dependence of the multiply scattered radiation. The modelled surface irradiances are computed for solar elevations of $\gamma = 15$, 20, 30, 45 and 60°. The relative airmass factor given in Eq. (2.2) is used since the curvature of the atmosphere and refraction are neglected in the model calculations. Relative airmass factors which are more appropriate for the actual direct solar irradiances observed at the surface are considered in Sec. 4.8.

4.1 Check of the algorithm

The algorithm described in Chapter 3 is used to derive the ozone column density from the modelled direct irradiances reaching the surface. The retrieval algorithm uses the SUSIM extraterrestrial solar spectrum (cf. Sec. 4.6); the Bass & Paur ozone absorption cross-section at 228 K (cf. Sec. 4.3); the analytical expression of Hansen & Travis for the molecular optical thickness (cf. Sec. 4.2); and assumes no wavelength dependence of the aerosol optical thickness. In Table 4.1 the retrieved ozone column densities obtained from the modelled surface irradiances are given for the MLS atmosphere with and without aerosol. Table 4.1 shows that the first estimate of the ozone column density is rather poor, especially for low solar elevations. However, successive iterations improve the results rapidly for all solar elevations. The retrieved ozone column densities for the clear atmosphere are in good agreement with the actual ozone

Table 4.1 Derived total ozone (in DU) for the MLS standard atmosphere with an ozone column density of 334 DU after subsequent iteration steps. The results are gives for 5 solar elevations and the wavelength combinations 302 & 306 and 306 & 310 nm.

no aerosol					
# iterations	$\gamma = 15°$	$\gamma = 20°$	$\gamma = 30°$	$\gamma = 45°$	$\gamma = 60°$
0	253 / 291	263 / 300	275 / 311	285 / 318	289 / 322
1	309 / 326	315 / 330	321 / 333	325 / 335	327 / 335
2	327 / 334	330 / 335	332 / 336	334 / 336	334 / 336
3	333 / 336	334 / 336	335 / 337	335 / 337	336 / 337
4	335 / 337	335 / 337	336 / 337	336 / 337	336 / 337
5	336 / 337	336 / 337	336 / 337	336 / 337	336 / 337
aerosol					
# iterations	$\gamma = 15°$	$\gamma = 20°$	$\gamma = 30°$	$\gamma = 45°$	$\gamma = 60°$
0	256 / 296	266 / 306	278 / 316	288 / 324	292 / 328
1	313 / 333	318 / 336	325 / 339	329 / 341	331 / 342
2	331 / 341	334 / 342	336 / 343	337 / 343	338 / 343
3	337 / 343	338 / 343	339 / 343	339 / 343	339 / 343
4	339 / 344	340 / 343	340 / 343	340 / 343	340 / 343
5	340 / 344	340 / 344	340 / 343	340 / 343	340 / 343

column density. The difference of 2 to 3 DU is the result of using the ozone absorption cross-section at a fixed temperature instead of using the temperature profile to account for the temperature dependence of the ozone absorption cross-section (cf. Sec. 4.3). The test case with aerosol gives ozone column densities that are slightly higher, since the spectral dependence of the aerosol optical thickness is partly attributed to ozone. The optical thicknesses for the MLS standard atmosphere at 302, 306 and 310 nm are, respectively, 2.481, 1.426 and 0.778 for ozone, 1.177, 1.112 and 1.052 for molecular scattering, 1.141, 1.134 and 1.128 for scattering by aerosol, and 0.097, 0.093 and 0.089 for absorption by aerosol. The aerosol optical thickness in this example is rather large, but its spectral variation, which hampers the algorithm, is small. The retrieval algorithm yields aerosol optical thicknesses of 0.008 at 302 & 306 nm and 0.005 at 306 & 310 nm for the model atmosphere without aerosol and 1.406 at 302 & 306 nm and 1.391 at 306 & 310 nm for the case with aerosol. These aerosol optical thicknesses differ from the actual values given above because errors in the ozone and molecular

optical thickness are also ascribed to the aerosol optical thickness.

The above results show that the ozone column density can be derived by the method given in Chapter 3. This retrieval algorithm takes attenuation by molecules and aerosol into account as well as the effect of the filter function. The presence of sulpherdioxide and nitrogen dioxide in the atmosphere model did not influence the retrieved ozone column densities. Even enhancing the sulpherdioxide contents by a factor of 100, which gave a total sulpherdioxide column of about 11 DU, did not show any significant effect. The total ozone obtained with the wavelength pair 302 & 306 nm are better than those obtained for 306 & 310 nm, since the signal of ozone is stronger at shorter wavelengths and it is therefore less influenced by attenuation by molecules and aerosol. The accuracy of the retrieval algorithm for the MLS atmosphere model with aerosol is about 2 to 3%. However, for actual measurements the observed irradiances at shorter wavelengths may introduce larger errors due to the low irradiance levels at these wavelengths and the larger fraction of diffuse radiation compared to longer wavelengths. The ozone retrieval for the MLW standard atmosphere shows the same behaviour as for the MLS atmosphere. The ozone column densities derived for the MLW atmosphere including aerosol differ about 1% from the actual value. If the aerosol optical thickness decreases with increasing wavelength the presence of aerosol will lead to an overestimation of the ozone column density.

4.2 Molecular optical thickness

The optical thickness of molecular scattering is defined as

$$b_{\lambda,mol} = \int_0^\infty \sigma_{\lambda,mol}(z) n(z) dz, \tag{4.1}$$

with $\sigma_{\lambda,mol}(z)$ the molecular scattering cross-section per molecule (in cm^2), $n(z)$ is the number of molecules per unit volume (in cm^{-3}), and z the altitude (in cm). Molecular scattering applies to molecules and particles much smaller than the wavelength of the radiation. The electromagnetic field incident at the molecule can then be assumed to be constant around the molecule. The incident field induces a dipole moment in the molecule. This oscillating dipole emits according to classical electromagnetic theory. The molecular scattering cross-section is then given by (cf. e.g. Lenoble 1993)

$$\sigma_{\lambda,mol}(z) = \frac{128\pi^5}{3\lambda_{cm}^4} \gamma_{mol}^2 \frac{6+3\rho_n}{6-7\rho_n}, \tag{4.2}$$

where ρ_n is the depolarization factor, λ_{cm} is the wavelength in cm and γ_{mol} is the molecular polarizability. The refractive index $m(z)$ of a gas containing $n(z)$ molecules per unit volume is related to the molecular polarizability by the Lorentz-Lorenz relation

$$\gamma_{mol} = \frac{3}{4\pi n(z)} \frac{(m(z)^2-1)}{(m(z)^2+2)}. \tag{4.3}$$

Equation (4.3) shows that $(m(z)^2-1)/(m(z)^2+2)$ varies proportional to the density so that it is convenient to introduce the refractive index m_s at standard pressure $P_s = 1013.25$ hPa and temperature $T_s = 288.15$ K according to

$$\frac{(m(z)^2-1)}{(m(z)^2+2)} = \frac{(m_s^2-1)}{(m_s^2+2)}\frac{n(z)}{n_s}, \tag{4.4}$$

with $n_s = 2.54743 \times 10^{19}$ cm^{-3}. Inserting Eqs. (4.3) and (4.4) in (4.2) gives for the molecular scattering cross-section the familiar expression (cf. Bucholtz 1995)

$$\sigma_{\lambda,mol}(z) = \frac{24\pi^3}{\lambda_{cm}^4 n_s^2}\frac{(m_s^2-1)^2}{(m_s^2+2)^2}\frac{6+3\rho_n}{6-7\rho_n}. \tag{4.5}$$

The number density $n(z)$ (in cm^{-3}) which occurs in Eq. (4.1) is related to the local pressure $P(z)$ (in hPa) and temperature $T(z)$ (in K) by the equation of state

$$P(z) = n(z)kT(z), \tag{4.6}$$

with $k = 1.38066 \times 10^{-19}$ the Boltzmann constant. The molecular scattering optical thickness can be calculated from Eq. (4.1) by using Eqs. (4.5) and (4.6) in combination with the refractive index of air according to Peck & Reeder (1972), i.e.

$$(m_s-1)\times 10^8 = \frac{5791817}{238.0185-\lambda_\mu^{-2}} + \frac{167909}{57.362-\lambda_\mu^{-2}}, \tag{4.7}$$

with λ_μ the wavelength in microns and using the wavelength dependent depolarization factor reported by Bates (1984) with a value of $\rho_n = 0.03178$ near 306 nm.

Equations (4.5) - (4.7) are used in the atmospheric model to calculate the scattering optical thickness of molecules. The approximate analytical expression of Hansen & Travis (1974) is used in the retrieval algorithm in order to avoid the use of temperature and pressure profiles for the computation of the molecular scattering optical thickness. This expression (cf. Eq. (2.5)) gives the optical thickness for molecular scattering as a function of wavelength and requires only the surface pressure as input. In Table 4.2 the optical thickness obtained with this approximate analytical expression is compared to the optical thicknesses for the MLS and MLW standard atmospheres calculated by the atmospheric model. Molecular scattering optical thicknesses that have been computed by using other analytical expressions that can be found in the literature are also listed. These alternative expressions are

$$b_{\lambda,mol} = \frac{P}{1013.25}1.518\times 10^{10}\lambda^{-4.08} \tag{4.8}$$

according to Leckner (1978),

$$b_{\lambda,mol} = \frac{P}{1013.25}1.221\left(\frac{300}{\lambda}\right)^{4.27} \tag{4.9}$$

Table 4.2 Molecular scattering optical thicknesses for the MLS and MLW standard atmospheres at 302, 306 and 310 nm and the results obtained with the analytical expressions.

model	$\lambda = 302$ nm	$\lambda = 306$ nm	$\lambda = 310$ nm
MLS	1.177	1.112	1.052
MLW	1.180	1.115	1.055
Hansen & Travis	1.174	1.110	1.050
Leckner	1.156	1.095	1.039
Green *et al.*	1.187	1.122	1.061
Bucholtz	1.181	1.116	1.055
No correction	0.000	0.000	0.000

after Green *et al.* (1980) and

$$b_{\lambda,mol} = \frac{P}{1013.25} 0.00650362 \lambda_{\mu}^{-(3.55212+1.35579\lambda_{\mu}+0.11563/\lambda_{\mu})} \tag{4.10}$$

according to Bucholtz (1995). Table 4.2 shows that the molecular scattering optical thicknesses obtained with the analytical expressions of Hansen & Travis (1974) and Bucholtz (1995) are close to those calculated for the MLS and MLW standard atmosphere. The molecular scattering optical thickness according to the expression of Leckner (1978) is slightly to low, whereas that of Green *et al.* (1980) is a little to high compared to the optical thicknesses computed with the atmospheric model.

The ozone column densities that have been derived by using the different analytical expressions for the molecular scattering optical thickness are given in Table 4.3 for the MLS and MLW standard atmospheres without aerosol. These results have been obtained for a solar elevation of 45° and the wavelength pairs 302 & 306 as well as 306 & 310 nm. The ozone column densities obtained by using the analytical expression of Hansen & Travis are slightly higher than the actual value for the MLS and lower for the MLW atmosphere. This is a result of the temperature dependence of the ozone absorption cross-section which is approximated in the retrieval algorithm by considering the ozone absorption cross-section at an average temperature (cf. Sec. 4.3). Green *et al*'s and Bucholtz' expressions for the molecular scattering optical thickness yield ozone column densities that are almost identical to the ones obtained by using the analytical expression of Hansen & Travis. The ozone column densities derived by using Leckner's expressions are slightly higher since the molecular scattering optical thickness was underestimated. Without a correction for the spectral attenuation of direct solar radiation by molecular scattering the ozone column densities obtained by the algorithm are overestimated (cf. Table 4.3). This because the spectral dependence

Table 4.3 The ozone column densities for the MLS and MLW standard atmospheres and those retrieved for these atmosphere models for the wavelength pairs 302 & 306 and 306 & 310 nm by using the different analytical expressions for the molecular scattering optical thickness.

model	MLS	MLW
Actual value	334	378
Hansen & Travis	336 / 337	376 / 375
Leckner	337 / 339	377 / 376
Green *et al*	336 / 336	376 / 374
Bucholtz	336 / 336	376 / 374
No correction	359 / 372	399 / 410

which results from molecular scattering is attributed to ozone and a wavelength independent optical thickness is ascribed to aerosol.

Table 4.3 shows that a correction for the attenuation of direct solar radiation by molecular scattering is needed in order to derive the ozone column density accurately. All analytical expressions for the molecular scattering optical thickness considered above give about equally good results for both wavelength pairs with errors in the retrieved ozone column densities of ± 1 DU. The analytical expression of Hansen & Travis will be used in the retrieval algorithm.

4.3 Ozone absorption cross-section

The ozone absorption cross-section depends on temperature. This dependence is given in Fig. 4.1 by using the experimentally established data from Bass & Paur (1984) and Paur & Bass (1984). They expressed the temperature of the ozone absorption cross-section at each wavelength in terms of a second order polynomial in temperature. Figure 4.1 shows that the absorption cross-section of ozone between 290 and 330 nm increases with temperature and this increase is relatively more for longer wavelengths. The temperature dependence of the ozone absorption cross-section is considered in the atmospheric model by using the profiles of temperature and ozone for the MLS and MLW standard atmospheres (Anderson *et al.* 1986). The ozone absorption optical thickness is calculated from these profiles by using

$$b_{\lambda,O_3} = \int_0^\infty \sigma_{\lambda,O_3}(T(z)) n_{O_3}(z) dz. \tag{4.11}$$

The influence of the temperature dependence of the ozone absorption cross-section is studied by applying the retrieval algorithm with ozone absorption cross-sections at different temperatures. The retrieved ozone column density as a function of the

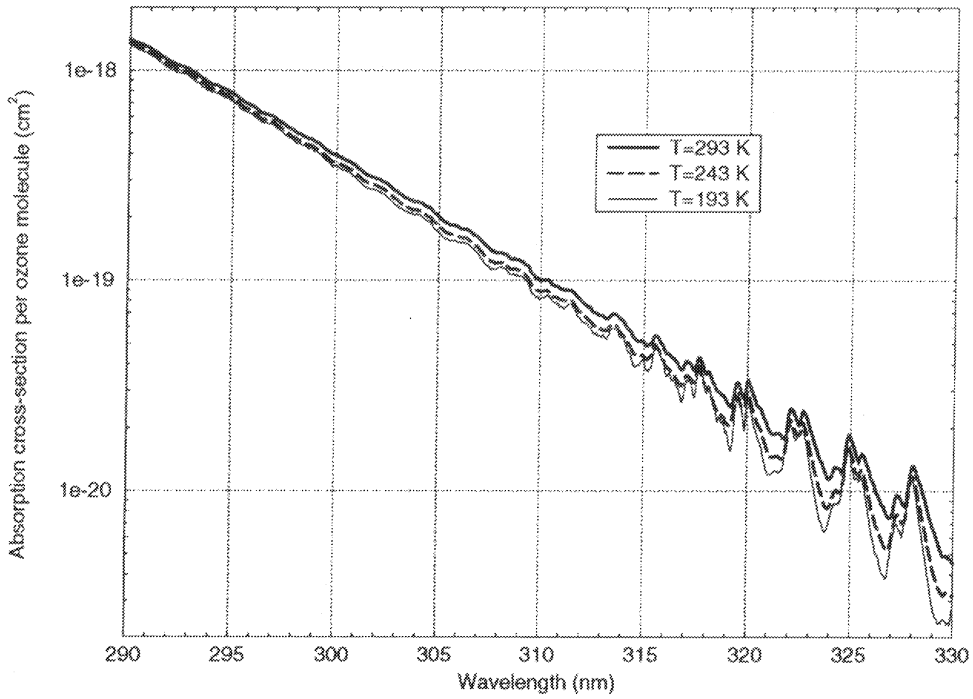

Figure 4.1 Spectral dependence of the absorption cross-section per ozone molecule σ_{λ,O_3} for different temperatures.

temperature of the ozone absorption cross-section are listed in Table 4.4 for the MLS and MLW atmosphere. The ozone column densities are obtained by using the 302 & 306 and 306 & 310 nm wavelength pairs. Since the actual ozone columns are 334 and 378 DU for the MLS and MLW atmospheres, respectively, Table 4.4 indicates that the best results are obtained by using the ozone absorption cross-section at T=233 K for the MLS and T=223 K for the MLW atmosphere. Clearly, this difference in the optimum temperature for the ozone absorption cross-section is a result of the lower temperatures in the MLW than the MLS standard atmosphere. Table 4.4 shows that a temperature difference of 10 K corresponds to a difference of about 4 DU in the ozone column density derived from the 302 & 306 nm wavelength pair, and 5 DU for the 306 & 310 nm wavelength pair. As could be expected from Fig. 4.1, the effect of the temperature dependence of the ozone absorption cross-section is larger for the wavelength combination at larger wavelengths. For both wavelength pairs a lower temperature leads to a larger ozone column density. The ozone column densities given in Table 4.4 are obtained for a solar elevation of 45°. The ozone column densities obtained for the other 4 solar elevations under consideration differ maximally about 2 DU for the MLS and 3 DU for the MLW atmosphere, respectively, from the tabulated results. The ozone column densities obtained for temperatures above the optimum temperature are smaller (larger) for smaller (larger) solar elevation, and vice versa for temperatures below the optimum temperature. The ozone column densities obtained for the 5 solar elevations differ only slightly for temperatures near the optimum temperature for the ozone absorption cross-section. The ozone absorption cross-section

Table 4.4 The ozone column densities (in DU) derived for the MLS and MLW standard atmospheres by using ozone absorption cross-sections at different temperatures (in K). The total ozone obtained with the 302 & 306 and 306 & 310 nm wavelength pairs are reported.

Temperature	MLS	MLW
193	345 / 352	387 / 392
203	343 / 348	383 / 387
213	340 / 344	381 / 382
223	337 / 339	378 / 377
233	334 / 334	374 / 372
243	331 / 329	370 / 366
253	328 / 324	366 / 361
263	324 / 319	362 / 355
273	320 / 314	358 / 349
283	315 / 308	353 / 343
293	311 / 303	348 / 337

at 228 K gives good results for both the MLS and MLW standard atmospheres, and is used in the retrieval algorithm.

4.4 Aerosol optical properties

Aerosol consists of small solid or liquid particles and is present even in clear atmospheres. The size of these particles ranges from nanometers to several microns. The aerosol which is most important in radiative processes are comparable to the wavelength of the radiation. Therefore, the aerosol optical properties have to be derived by solving the Maxwell equations. The solution depends on the refractive index, shape and size distribution of the particles. Generally, aerosol is assumed to consist of homogeneous spheres so that the solution of the Maxwell equations can be obtained from the so-called Mie theory (cf. e.g. Bohren & Huffman 1983). The spectral aerosol optical properties used in the atmospheric model have been calculated with Mie theory by using the refractive indices and size distributions of the basic aerosol models reported by the Radiation Commission of IAMAP (1986). The vertical distribution of the aerosol is also taken from this standard atmosphere. The spectral aerosol optical thickness that is thus obtained by the atmospheric model is used in the numerical simulations to test the retrieval algorithm (cf. Sec. 4.1).

The spectral dependence of the aerosol optical thickness is generally expressed in

Table 4.5 The ozone column densities (in DU) derived for the MLS standard atmosphere by using different coefficients in Ångström's turbidity formula for the aerosol optical thickness. The total ozone obtained with the 302 & 306 and 306 & 310 nm wavelength pairs are reported. Note that the atmospheric model including aerosol yielded 340 / 343 DU and using Green *et al.*'s expression gave 337 / 338 DU.

α	$\beta = 0.1$	$\beta = 0.2$	$\beta = 0.3$	$\beta = 0.4$	$\beta = 0.5$
0.0	336 / 337	336 / 337	336 / 337	336 / 337	336 / 337
0.8	337 / 338	338 / 340	339 / 341	340 / 343	341 / 345
0.9	337 / 339	338 / 341	340 / 343	341 / 345	342 / 347
1.0	338 / 339	339 / 342	341 / 344	342 / 347	344 / 349
1.1	338 / 340	340 / 343	342 / 346	344 / 349	346 / 352
1.2	338 / 340	341 / 344	343 / 348	345 / 352	348 / 356
1.3	339 / 341	342 / 346	345 / 351	348 / 355	350 / 360
1.4	339 / 342	343 / 348	346 / 354	350 / 359	354 / 365
1.5	340 / 343	344 / 350	349 / 357	353 / 364	357 / 371
1.6	341 / 345	346 / 353	351 / 361	356 / 370	361 / 378
1.7	342 / 346	348 / 356	354 / 366	360 / 376	366 / 386
1.8	343 / 348	350 / 360	358 / 372	365 / 384	372 / 395

terms of Ångström's turbidity formula (cf. e.g. Iqbal 1983)

$$b_{aer} = \beta \left(\frac{1000}{\lambda} \right)^{\alpha} . \tag{4.12}$$

In this formula, β is called Ångström's turbidity coefficient and represents the amount of aerosol present in the atmosphere. It varies between 0.0 and 0.5. A good average value for the wavelength exponent $\alpha = 1.3 \pm 0.5$. Green *et al.* (1974) use the expression

$$b_{aer} = 0.41 \left(\frac{300}{\lambda} \right)^{0.576} , \tag{4.13}$$

which is outside the range of Ångström's turbidity formula.

In this section the sensitivity of the retrieval algorithm to the assumption of a wavelength independent aerosol optical thickness is investigated. For that purpose the analytical expressions are used to calculate the direct solar radiation attenuated by aerosol. This is done by using various values for the turbidity coefficient β and the wavelength exponent α in Ångström's turbidity formula (cf. Eq.(4.12)). The derived ozone column densities are reported in Table 4.5 for a solar elevation of 45°. These results show that the derived ozone column density deteriorates with increasing aerosol loading and exponent and this is worse for the longer wavelength combination. The

presence of wavelength dependent aerosol enhances the derived ozone column density because the wavelength dependency is partly ascribed to ozone. This enhancement is slightly higher for lower solar elevations. The effect of aerosol is stronger for the 306 & 310 wavelength combination because the relative contribution of the aerosol optical thickness to the total optical thickness is larger at longer wavelengths. For clear atmospheres with $\beta = 0.1$ an overestimation of up to 6 DU for the 302 & 306 nm and 10 DU for the 306 & 310 nm wavelength combination are obtained over the full range of the wavelength exponent of Ångström's turbidity formula. The aerosol considered in the atmospheric model (cf. Sec. 4.1) corresponds with Ångström's turbidity formula for a wavelength exponent α less than 0.8 and a turbidity coefficient $\beta \approx 0.5$. The analytical expression of Green *et al.* has a wavelength exponent $\alpha = 0.576$ and turbidity coefficient $\beta \approx 0.8$. Aerosol having such a low wavelength dependency has only a small effect on the derived ozone column density, even if the aerosol contents is rather large. The overestimation is about 5 and 9 DU for the 302 & 306 and 306 & 310 nm wavelength combination, respectively, when aerosol with $\alpha = 0.8$ and $\beta = 0.5$ is considered. However, in cases with high aerosol contents (large β) in combination with a large wavelength dependence of the aerosol (large α) the overestimation of the derived ozone column density is large. Note that in such situations the above analytical expressions could be used to correct the observed direct solar irradiance reaching the surface for the spectral attenuation by aerosol. The Brewer spectrophotometer derives the ozone column density using a combination of the direct sun measurements at 4 wavelength bands in the UVB. The combination is chosen such that attenuation by SO_2 and a linear wavelength dependence of attenuation by aerosol are eliminated.

The presence of aerosol may lead to large overestimations of the ozone column density. However, if the atmospheric aerosol contents is low or if the spectral dependence of the aerosol is small, the overestimation is less than about 5 DU for the 302 & 306 and less then 10 DU for the 306 & 310 wavelength combination. The effect of the aerosol on the retrieved ozone column density increases with increasing wavelength.

4.5 Filter function

In this section the sensitivity of the algorithm to the filter function is investigated. The direct solar radiation that reaches the surface has been calculated by using the 'actual' filter function presented in Fig. 4.2. This curve shows the filter function of the Kipp & Zonen' narrow band UVB radiometer which is operated at KNMI (cf. Kuik & Kelder 1994). The retrieval algorithm has been applied on the irradiances that have been obtained with this filter function, but in the retrieval algorithm other filter functions are also considered. The block, triangle and Gaussian filter functions with a different shape, but the same central wavelength λ_c, width w and maximum sensitivity F_{max} as

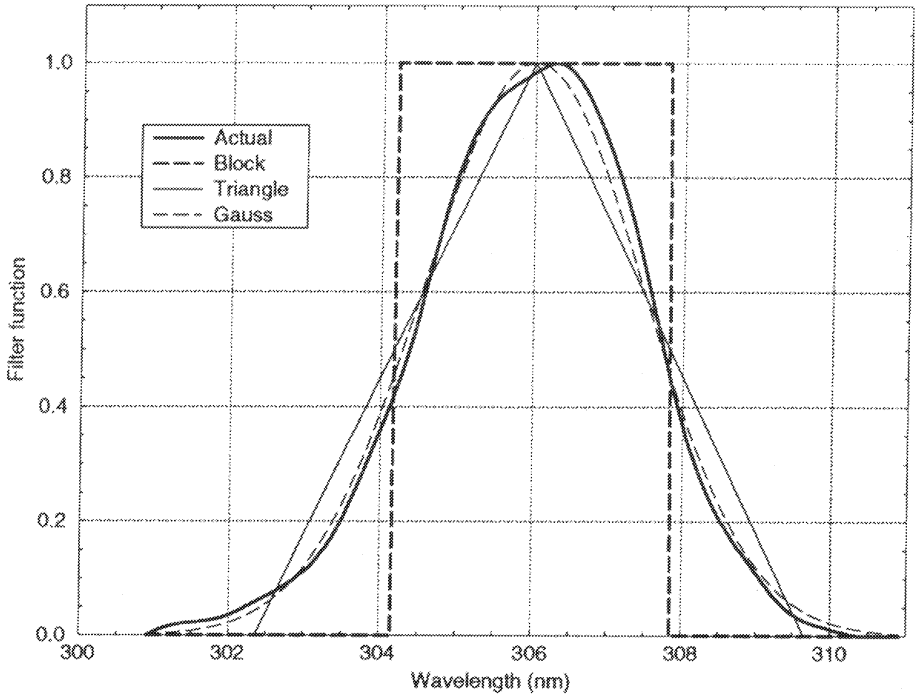

Figure 4.2 Spectral dependence of the filter functions F_λ with central wavelength $\lambda_c = 306$ nm, width $w = 3.65$ and maximum sensitivity $F_{max} = 1$. The various curves have a different shape, but identical central wavelength, width and maximum sensitivity.

the actual filter are used for this purpose. Here the block filter function is defined by

$$F_\lambda = F_{max} \qquad \text{if} \qquad \lambda_c - \frac{w}{2} \leq \lambda \leq \lambda_c + \frac{w}{2} \tag{4.14}$$

and zero elsewhere, the triangular filter by

$$F_\lambda = F_{max}\left(1 - \frac{|\lambda - \lambda_c|}{w}\right) \qquad \text{if} \qquad \lambda_c - w \leq \lambda \leq \lambda_c + w \tag{4.15}$$

and zero elsewhere, and the Gaussian filter by

$$F_\lambda = F_{max} \exp\left[-\pi\left(\frac{\lambda - \lambda_c}{w}\right)^2\right] \tag{4.16}$$

for all wavelengths. In addition to these alternative filter functions, the actual filter is used, but with a different width or central wavelength. Note that the filter functions for the two wavelengths used in the retrieval algorithm need to be calibrated, since an uncertainty in the maximum sensitivity of one of the filter functions leads directly to an error in the derived ozone column density.

The ozone column densities that have been derived by using the various alternative filter functions are listed in Table 4.6 for the MLS standard atmosphere without aerosol, 5 solar elevations and the wavelength pairs 302 & 306 and 306 & 310 nm.

Table 4.6 The ozone column densities (in DU) for the MLS standard atmosphere and 5 solar elevations derived by using different filter functions.

Filter	$\gamma = 15°$	$\gamma = 20°$	$\gamma = 30°$	$\gamma = 45°$	$\gamma = 60°$
Actual	336 / 337	336 / 337	336 / 337	336 / 337	336 / 337
Block	302 / 331	309 / 333	314 / 336	318 / 338	319 / 340
Triangle	347 / 341	346 / 340	344 / 340	341 / 339	340 / 339
Gaussian	345 / 341	342 / 340	340 / 339	338 / 338	337 / 338
Smaller 5%	328 / 334	329 / 335	331 / 336	332 / 337	332 / 337
Broader 5%	344 / 340	343 / 339	341 / 338	341 / 337	340 / 337
One shifted −0.1 nm	345 / 346	345 / 346	345 / 347	345 / 347	345 / 347
One shifted +0.1 nm	328 / 328	328 / 328	328 / 327	328 / 327	328 / 327
Both shifted −0.1 nm	331 / 333	331 / 333	330 / 333	329 / 334	328 / 334
Both shifted +0.1 nm	341 / 341	342 / 340	342 / 340	343 / 339	343 / 339

Table 4.6 shows that the effect of the filter function depends on the solar elevation and the wavelength pair. Generally, the results for the 306 & 310 nm wavelength pair are less dependent on the filter function than those for the 302 & 306 nm wavelength pair. Table 4.6 also shows that the sensitivity to the filter function is generally larger for smaller solar elevations. The block filter function underestimates the ozone column density by about 15-40 DU for the 302 & 306 nm wavelength pair and about 5 DU for the 306 & 310 nm wavelength pair. Using a triangular or Gaussian filter shape improves the results and leads to overestimations of the ozone column density by up to 10 and 5 DU for the 302 & 306 and 306 & 310 nm wavelength pairs, respectively. A narrower filter yields an ozone column density that is about 8 and 4 DU to small for the 302 & 306 and 306 & 310 nm wavelength pairs, respectively, whereas the ozone column density is to high for a broader filter. The width of the filter has almost no influence for the 306 & 310 nm wavelength pair and solar elevations larger than 45°. Shifting one or both filters of the wavelength pair has almost the same effect for both wavelength pairs and all solar elevations. Shifting the filter of the largest wavelength in the pair +0.1 nm increases the ozone column density by about 10 DU, whereas a shift of −0.1 nm reduces the ozone column density by 10 DU. Shifting both wavelengths +0.1 nm reduces the ozone column density by about 5 DU and shifting them −0.1 nm increases the results by 5 DU.

The ozone column densities derived by using the retrieval algorithm presented in Chapter 3 depend on the filter function of the instrument. This dependence is generally most pronounced for the 302 & 306 nm wavelength pair and at small solar elevations. In these situations the bandwidth effect of the filter function is also largest. Errors of 5-10 DU in the retrieved ozone column densities occur when using a realistic shape

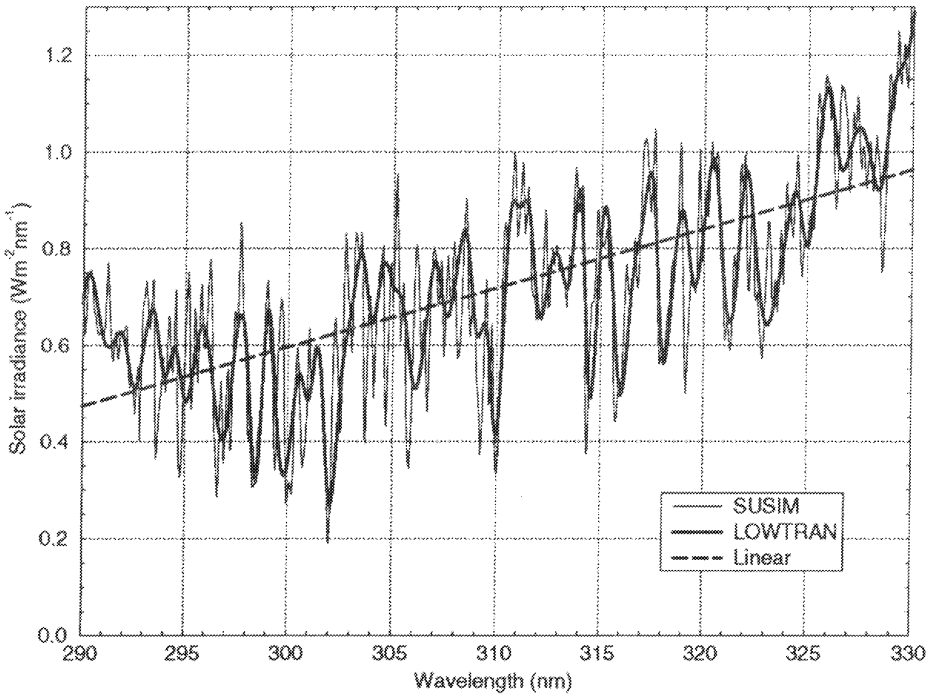

Figure 4.3 Spectral dependence of the solar irradiance S_λ incident at the top of the atmosphere. Presented are the SUSIM and LOWTRAN 7 solar spectra and a linear fit to the SUSIM spectrum.

for the filter function with the correct central wavelength and width. Using a block shaped filter function with the correct parameters instead, resulted in errors up to 30 DU. Therefore, the spectral dependence of the filter function has to be measured accurately.

4.6 Solar irradiance

In this section the sensitivity of the results to the incident solar irradiance is investigated. The solar irradiance incident at the top of the atmosphere varies in time due to seasonal variation of the distance between the sun and Earth and due to variations in the radiation emitted by the sun during the solar rotation and the solar cycle. These variations need to be considered if absolute irradiances are required for the determination of the aerosol optical thickness. The variations in incident solar irradiance related to the seasonal variations in the distance between the sun and Earth reach values up to about 3 %, but these variations can easily be taken into account by using the empirical equation (cf. Spencer 1971)

$$S_\lambda(J) = S_\lambda \left[1.000110 + 0.034221 \cos\left(\frac{2\pi(J-1)}{365}\right) + 0.001280 \sin\left(\frac{2\pi(J-1)}{365}\right) + 0.000719 \cos\left(\frac{4\pi(J-1)}{365}\right) + 0.000077 \sin\left(\frac{4\pi(J-1)}{365}\right) \right] \quad (4.17)$$

Table 4.7 The ozone column densities (in DU) for the MLS standard atmosphere and 5 solar elevations derived by using different solar spectra.

spectrum	$\gamma = 15°$	$\gamma = 20°$	$\gamma = 30°$	$\gamma = 45°$	$\gamma = 60°$
SUSIM	336 / 337	336 / 337	336 / 337	336 / 337	336 / 337
LOWTRAN 7	337 / 342	336 / 341	333 / 341	330 / 341	327 / 341
Linear	332 / 342	333 / 340	338 / 339	344 / 337	350 / 335
SUSIM −0.1 nm	337 / 335	337 / 335	337 / 335	338 / 334	339 / 334
SUSIM +0.1 nm	336 / 338	335 / 338	335 / 339	334 / 339	333 / 339

which relates the solar irradiance $S_\lambda(J)$ at Julian day J to the mean solar irradiance S_λ where the Julian day is the day of the year counted from 1 to 365 (or 366) starting on January 1. The variations in the radiation emitted by the sun due to variations in solar rotation and activity are about 1 % and do not alter the spectral distribution of the solar irradiance in the UVB. Note that only variations in the spectral distribution of the solar radiation directly affect the derivation of the ozone column density.

In practice, the extraterrestrial solar irradiance is obtained with the so-called Langley method. For that purpose the natural logarithm of the observed direct solar irradiance at the surface is plotted as a function of the airmass factor and extrapolated to zero airmass. Thus the solar irradiance which would be observed by the instrument at the top of the atmosphere is obtained. However, note that this zero airmass irradiance is weighted with the filter function of the instrument and furthermore, that it may be affected by the presence of diffuse radiation or variations in the atmospheric attenuation during the course of the day over which the observations at various solar elevations have been performed. Therefore, such measurements are generally made from high-altitude observatories with relatively clear and stable atmospheres. In this section the irradiances that reach the detector have been calculated by using the SUSIM spectrum for the solar radiation incident at the top of the Earth atmosphere (VanHoosier *et al.* 1988). Different solar spectra have been considered for the retrieval of the ozone column density (cf. Fig. 4.3). These alternative solar spectra are the LOWTRAN 7 spectrum with a spectral resolution of 5 cm^{-1}, a linear fit to the SUSIM spectrum between 290 and 330 nm and the SUSIM spectrum, but shifted 0.1 nm to both smaller and larger wavelengths.

Table 4.7 presents ozone column densities that have been obtained by using the various spectra for the solar irradiance incident at the top of the atmosphere. Again the wavelength pairs 302 & 306 and 306 & 310 nm are considered for the MLS standard atmosphere without aerosol at 5 solar elevations. The differences in ozone column densities obtained by using the various solar spectra are not so large since the broadness of the filter function eliminates the influence of individual lines in the solar spectrum.

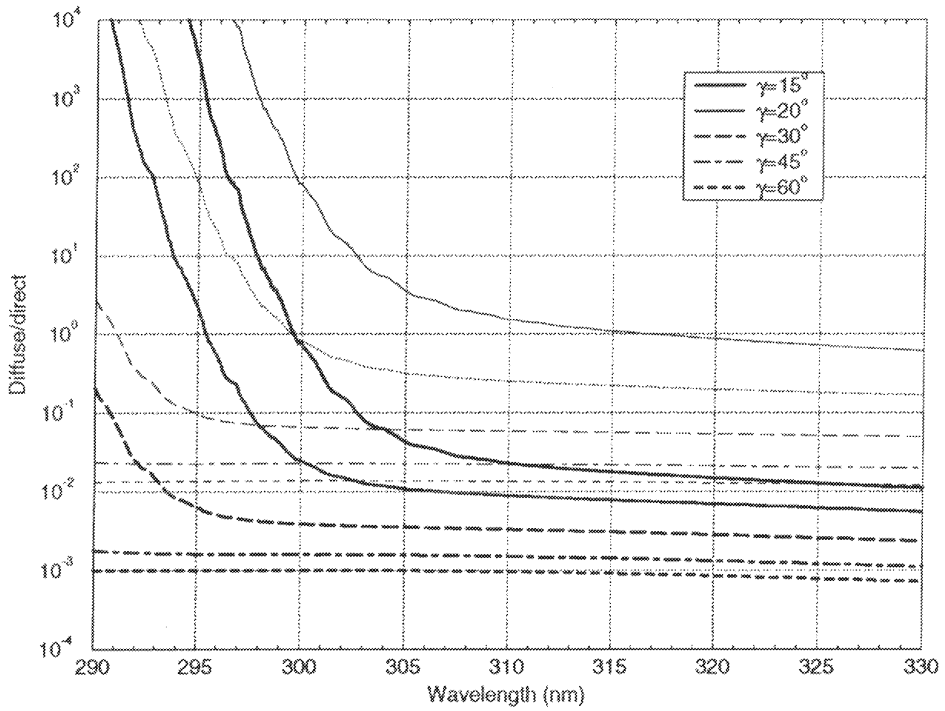

Figure 4.4 Spectral dependence of the ratio of diffuse to direct irradiance at the surface of the MLS standard atmosphere for 5 solar elevations. Thick lines indicate the curves for the case without aerosol and thin lines the case including aerosol.

The LOWTRAN 7 solar spectrum yields ozone column densities which are typically 5 DU to high for the 306 & 310 wavelength pair at all 5 solar elevations. The 302 & 306 wavelength pair gives good results for low solar elevations, but underestimates the ozone column density by about 10 DU for $\gamma = 60°$. Using the linear fit to the SUSIM data as the solar spectrum gives results similar to those of the LOWTRAN 7 spectrum for the 306 & 310 nm wavelength pair, but the results are worse for the 302 & 306 nm wavelength pair where ozone column densities are about 5 DU to small at low solar elevations and 15 DU to large for high solar elevations. A wavelength shift of the incident solar spectrum by ± 0.1 nm yields differences in the ozone column densities of about 5 DU. A shift of -0.1 nm yields higher ozone column densities for the 302 & 306 wavelength pair and lower ozone column densities for the 306 & 310 wavelength pair. The $+0.1$ nm shift gives the opposite effect. A behaviour similar to that reported above was also found for the MLW standard atmosphere.

The sensitivity of the derived ozone column densities to the spectrum of the incident solar irradiance is generally largest for the 302 & 306 wavelength pair at high solar elevations. The maximum error is about 10 DU.

4.7 Diffuse radiation

Here the role of diffuse, i.e. scattered, radiation is studied. This scattered radiation may contribute to the radiation in the direction of the incident solar radiation. The

Table 4.8 The ozone column densities for the MLS standard atmosphere and 5 solar elevations obtained by considering both direct and diffuse radiation. The standard atmosphere with and without aerosol is considered.

			without aerosol		
opening angle	$\gamma = 15°$	$\gamma = 20°$	$\gamma = 30°$	$\gamma = 45°$	$\gamma = 60°$
0°	336 / 337	336 / 337	336 / 337	336 / 337	336 / 337
1°	335 / 336	336 / 337	336 / 337	336 / 337	336 / 337
2°	332 / 335	336 / 336	336 / 337	336 / 337	336 / 337
3°	326 / 333	335 / 336	336 / 337	336 / 337	336 / 337
4°	320 / 331	335 / 336	336 / 336	336 / 337	336 / 337
5°	313 / 328	334 / 335	336 / 336	336 / 337	336 / 337
			with aerosol		
opening angle	$\gamma = 15°$	$\gamma = 20°$	$\gamma = 30°$	$\gamma = 45°$	$\gamma = 60°$
0°	340 / 344	340 / 344	340 / 343	340 / 343	340 / 343
1°	282 / 318	337 / 341	340 / 343	340 / 343	340 / 343
2°	246 / 290	330 / 336	340 / 343	340 / 343	340 / 343
3°	234 / 277	322 / 331	339 / 342	340 / 343	340 / 343
4°	228 / 271	316 / 326	338 / 341	340 / 343	340 / 343
5°	226 / 268	312 / 322	338 / 340	339 / 342	339 / 342

diffuse radiation observed by the instrument during a direct sun measurement may affect the derivation of the ozone column density. The diffuse radiation is a result of scattering by molecules or aerosol. The aerosol loading in the atmosphere and its optical properties are variable. Therefore, the contribution of the multiply scattered radiance in the direction of the incident solar radiation is studied using spectral radiances calculated with the radiative transfer model coupled to the MLS standard atmosphere without and with aerosol. This radiance is multiplied with the solid angle determined by the opening angle of the instrument to simulate the irradiance incident at the instrument. Figure 4.4 illustrates the contribution of diffuse irradiance observed by an instrument with an opening angle of 2° as a function of wavelength. The results show that the relative amount of diffuse radiation decreases with increasing solar elevation and with increasing wavelength. The presence of aerosol enhances the fraction of diffuse radiation. The spectral dependence of the relative contribution of diffuse radiation near 306 nm is high for solar elevation less than 20° and increases rapidly at shorter wavelengths. This spectral dependence introduced by scattered radiation affects the derivation of the ozone column density.

The simulated scattered irradiance at the surface is added to the modelled direct solar irradiance at the surface and weighted with the actual filter function. The ozone column density is derived from this combined signal. The ozone column densities obtained for opening angles of 0 to 5° are presented in Table 4.8. The results show that diffuse radiation only affects the derivation of the ozone column density at low solar elevations. For solar elevation of 30° and larger the derived ozone column densities are not influenced by diffuse radiation for the aerosol free atmosphere and are underestimated maximally about 2 DU for the atmosphere including aerosol. The differences are maximally 2 and 30 DU for a solar elevation of 20° for the cases without and with aerosol, respectively. The ozone column densities derived with direct and diffuse radiation incident at the detector differ considerably from those obtained for direct radiation only for a solar elevation of 15°. The effect of diffuse radiation for a solar elevation of 15° in the aerosol free atmosphere is maximally about 25 DU for the 302 & 306 nm wavelength pair and about 10 DU for the 306 & 310 nm wavelength pair. The atmosphere containing aerosol has errors of about 60 and 30 DU for the 302 & 306 and 306 & 310 wavelength combination, respectively, even for an opening angle of 1°. The amount of direct radiation incident at the surface is small for low solar elevations due to the large optical path. Because scattered radiation has a shorter optical path, it is less attenuated, and it may therefore contribute significantly to the radiation in the direction of the incident solar radiation. This relative contribution of diffuse radiation is larger at smaller wavelengths. The ozone column densities derived with the 302 & 306 nm wavelength pair are therefore more influenced by diffuse radiation than those of the 306 & 310 nm wavelength pair. Diffuse radiation leads to an underestimation of the ozone column density because the increase of radiation due to scattering is relative larger at smaller wavelengths whereas the presence of ozone leads to a reduction of radiation that is relative larger at smaller wavelengths. This underestimation caused by diffuse radiation increases with increasing opening angle of the instrument. Note that the rural aerosol type considered in the atmosphere model has about the same spectral attenuation as the urban aerosol type, but rural aerosol absorbs less radiation than urban aerosol. Therefore, less diffuse radiation will be present in the standard atmosphere with urban aerosol. Also note that the radiation scattered by aerosol generally decreases with increasing scattering angle. Hence the amount of diffuse radiation incident at the instrument is generally less than the radiation scattered in the direction of the incident solar radiation times the solid angle determined by the opening angle of the instrument.

Diffuse radiation leads to an underestimation of the derived ozone column density, especially at low solar elevations. This effect increases with increasing opening angle of the instrument and is enhanced by the presence of aerosol. The measurements may in a first approximation be corrected for diffuse radiation resulting from scattering by both molecules and aerosol by subtracting the corresponding measurements close to, but not including the direct solar radiation, from it. The so-called focused sun

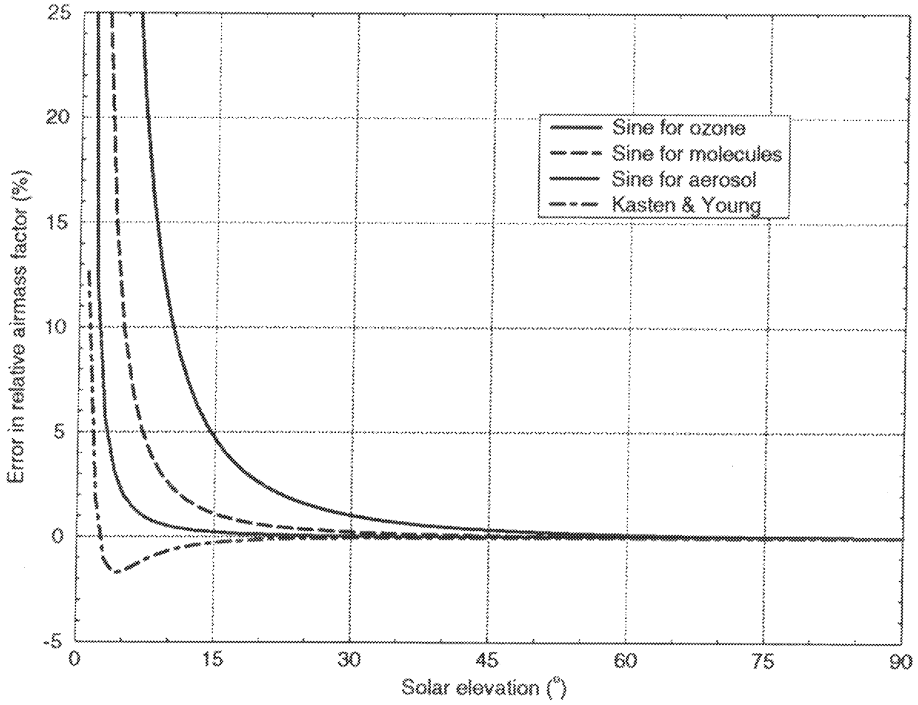

Figure 4.5 The error (in %) in the relative airmass factor compared to the values calculated from Eq. (4.20) for different atmospheric constituents as a function of solar elevation.

observations with the Brewer spectrophotometer use the same correction for diffuse radiation (cf. Josefsson 1992).

4.8 Relative airmass factor

For low solar elevations the optical path through the atmosphere is not related to the vertical optical path according to Eq. (2.2) due to the curvature of the atmosphere and refraction. This effect can not be studied with the plane-parallel atmosphere model considered in the numerical simulations. Therefore expressions for the relative airmass factor which account for curvature and refraction are compared with the relative airmass factor for plane-parallel atmospheres given in Eq. (2.2). Such a comparison shows for which solar elevations the plane-parallel assumption of the relative airmass factor is valid and gives the sensitivity of the results to uncertainties in the solar elevation and the various expressions for the airmass factor. The general expression for the relative airmass factor between altitudes z_0 and z_1 of an atmospheric constituent with density n at altitude z for a spherical atmosphere including refraction may be written as (cf. McClatchey 1972)

$$m_r = \left[\int_{z_0}^{z_1} n(z)dz\right]^{-1} \int_{z_0}^{z_1} \left[1 - \left(\frac{R+z_0}{R+z}\right)^2 \left(\frac{m(z_0)}{m(z)}\cos\gamma\right)^2\right]^{-1/2} n(z)dz \qquad (4.18)$$

where m is the refractive index of air (cf. Eq. (4.7)) and R is the radius of the Earth. The relative airmass factor can be calculated using the above expression if the profiles of pressure, temperature and the constituent are known. Such computations are used to construct empirical expressions. An empirical relative airmass factor for scattering by molecules which takes the curvature and refraction in the atmosphere into account is given by

$$m_r = \frac{1}{\sin\gamma + a(\gamma + b)^{-c}}, \tag{4.19}$$

where $a = 0.50572$, $b = 6.07995°$ and $c = 1.6264$ according to Kasten & Young (1986). A useful approximate expression can also be obtained from Eq. (4.18) by assuming that the attenuating constituent is only present at a certain altitude h and ignoring refraction since the refractive index of air near the surface is only 1.00029 at 306 nm (cf. Eq. (4.7)). The relative airmass factor at the surface of a spherical atmosphere with attenuation occurring at altitude h is then given by (cf. Green *et al.* 1974)

$$m_r = \frac{1}{\sqrt{1 - (\frac{R\cos\gamma}{R+h})^2}}. \tag{4.20}$$

Here R is the radius of the Earth, i.e. 6370 km, and the height h where attenuation occurs is typically 22 km for absorption by ozone, 5 km for scattering by molecules and 1 km for aerosol. The assumption that the altitude h is much smaller than the radius of the Earth R can be used to write Eq. (4.20) as

$$m_r = \frac{1 + h/R}{\sqrt{\sin^2\gamma + 2h/R}}. \tag{4.21}$$

Note that for very small values of h Eqs. (4.20) and (4.21) reduces to Eq. (2.2).

In Fig. 4.5 the error in relative airmass factors obtained by using different expressions are presented as a function of solar elevation. The relative airmass factors are almost identical to that of the plane-parallel approximation for high solar elevations. At $\gamma = 15°$ the sine overestimates the other 3 relative airmass factors by about 5% for ozone absorption, 1% for molecular scattering and 0.25% for aerosol. The differences are 10, 3 and 0.5%, respectively, at $\gamma = 10°$ and 21, 5 and 1% at $\gamma = 7°$, respectively, for ozone, molecules and aerosol. The curvature of the atmosphere must be taken into account for solar elevations less than 30°, because the differences in the relative airmass factor due to ozone absorption are more than 1%. Therefore, the relative airmass factor used for the retrieval of ozone columns from observations is not the one given by Eq. (2.2), but Eq. (4.20) with different layer heights for attenuation by ozone, molecules and aerosol. The results for molecules obtained by using Eq. (4.20) differ less than 1% from the values obtained by using Eq. (4.19) except for solar elevations below 5°.

Chapter 5

Conclusions and outlook

A new algorithm is presented which derives the ozone column density from direct sun measurements at two wavelengths in the UVB. A correction is applied for the spectral attenuation by molecular scattering and the effect of aerosol is assumed to be independent of wavelength. The ozone column density can then be derived by using the spectral dependence of the ozone absorption cross-sections in combination with the spectrum of the incident solar radiation. The retrieval algorithm uses the filter function of the instrument in order to correct for its spectral sensitivity. This correction is needed for measurements at short wavelengths with a relatively large width of the filter function, typically $w = 5$ nm at $\lambda_c = 320$ nm, $w = 3$ nm at $\lambda_c = 315$ nm, $w = 1$ nm at $\lambda_c = 310$ nm and $w = 0.5$ nm at $\lambda_c = 305$ nm. The correction depends on both the ozone column and the solar elevation, individually. If the instrument is calibrated absolutely, the aerosol optical thickness can also be derived.

The sensitivity of the retrieved ozone column density to various assumptions and uncertainties in the algorithm has been investigated by applying the algorithm to simulated direct sun irradiances calculated with an atmospheric model. These simulations show that: (i) the ozone column density can be derived from direct sun measurements at 2 wavelengths bands in the UVB using the above mentioned algorithm which accounts for the filter function of the instrument; (ii) the wavelength dependence of attenuation by molecular scattering must be taken into account, but various analytical expressions which can be used for this correction give good results; (iii) the temperature dependence of the ozone absorption cross-section has been taken into account by adopting an averaged temperature of 228 K resulting in an accuracy of about ± 3 DU; (iv) the presence of aerosol generally leads to an overestimation of the ozone column density which is worse at longer wavelengths because of the larger relative attenuation by aerosol at longer wavelengths. A low atmospheric aerosol content or a small wavelength dependence of the attenuation by aerosol gives an overestimation less than about 5 DU for the 302 & 306 and less then 10 DU for the 306 & 310 wavelength combination. (v) the filter function of the instrument has to be accurately known, especially for the 302 & 306 nm wavelength pair and at low solar elevations where errors of about 10 DU may occur; (vi) the sensitivity to the incident solar radiation is relatively small due to the width of the filter function, but

is maximally 10 DU for the 302 & 306 nm wavelength pair at high solar elevations; (vii) diffuse radiation in clear atmospheres has only an effect at low solar elevations in combination with a large opening angle of the instrument. The presence of aerosol deteriorates the results significantly. Diffuse radiation lead to an underestimation of the ozone column density because scattering has a relatively larger contribution at shorter wavelength and the effect is therefore most pronounced for the 302 & 306 nm wavelength pair; (viii) the curvature of the atmosphere must be taken into account for solar elevations below 30°. Note that the results of the sensitivity study reported above have been obtained by varying each of the parameters individually. In practice all uncertainties need to be considered together. Therefore, the overall error is not the sum of the individual errors, but because of cancelling of errors it will be less. Furthermore, the accuracy may be improved by performing measurements during clear situation, for high solar elevations and using an instrument with a small opening angle.

An instrument similar to the one considered in this work is being developed in a cooperation between KNMI and Kipp & Zonen. Although the sensitivity tests performed here provide useful information on the algorithm and the choice of various parameters, the actual test of the ozone column density retrieval algorithm needs to be done in the field. A first prototype of this instrument built by Kipp & Zonen is available and has been tested and calibrated at KNMI. This summer extensive measurements will be performed with the filter instrument. The calculated ozone column densities will be compared with values obtained with a Brewer spectrophotometer operated at KNMI.

The retrieval algorithm presented in this report can also be applied to the narrow band UVB and UVA direct sun radiometers which are operated at KNMI. The UVA wavelength band (λ_c = 368 nm and w = 10 nm) can be used to calculate the aerosol optical thickness and ozone can be derived in the UVB (λ_c = 306 nm and w = 2 nm). Because the two wavelength bands are far apart, the assumption of a wavelength independent aerosol optical thickness cannot be made, but instead Ångström's turbidity formula has to be used to relate the aerosol optical thickness in the UVB band to the one derived in the UVA. However, these instruments have the advantage that they are calibrated absolutely, proved to be stable and perform measurements that are archived every 10 seconds. In addition, the Langley method can be apllied in the UVA in order to get the extraterrestrial irradiance as observed by the instrument. The retrieval algorithm can also be applied to the Brewer direct sun measurements at 5 narrow wavelength bands in the UVB (λ_c = 306.3, 310.1, 313.5, 316.8 and 320.1 nm and w = 0.6 nm). The retrieval algorithm presented in this report can be compared to the direct sun algorithm used by the Brewer. A sensitivity study similar to the one presented in this report, but for the direct sun ozone column density retrieval algorithm of the Brewer instrument could also be performed.

Acknowledgements

The work presented in this report has been triggered by the demand of the Dutch 'ozonmeter' group for an ozone column density retrieval algorithm for their filter instrument. The 'ozonmeter' group, which consists of D.A. Kraijenhoff van de Leur (Rotary Club), F. Kuik (KNMI), J. van Heugten (van Maerlantlyceum Eindhoven), P. Hofschreuder (Wageningen Agricultural University), L. van Wely (Kipp & Zonen) and myself, is developing a filter-spectrophoto-ozonometer for educational purposes. Stimulating discussion in the 'ozonmeter' group is gratefully acknowledged. It is a pleasure to thank Leo van Wely for constructing a first prototype of the filter instrument and Foeke Kuik for performing the calibration and the first test measurements with the aid of his students Frank Helderman and Gert Jan Lieftink. I am indebted to Piet Stammes (KNMI) for providing the atmospheric model that is used for perfoming the numerical simulations. Furthermore, I wish to thank Foeke Kuik, Piet Stammes, Dirk Kraijenhoff and Johan de Haan (Free University Amsterdam) for useful suggestions and comments on an earlier version of this report.

References

Anderson, G.P., S.A. Clough, F.X. Kneizys, J.H. Chetwind and E.P. Shettle: "AFGL Atmospheric Constituents Profiles (0-120km)", Air Force Geophysics Laboratory, AFGL-TR-86-0110, Environmental Research Papers No. 954, Hanscom, MA (1986)

Basher, R.E.: "The Effect of Bandwidth of Filter Instrument Total Ozone Accuracy", *J. Appl. Meteorology* **16**, 803-811 (1977)

Basher, R.E. and W.A. Matthews: "Problems in the Use of Interference Filters for Spectrophotometric Determination of Total Ozone", *J. Appl. Meteorology* **16**, 795-802 (1977)

Bass, A.M. and R.J. Paur: "The Ultraviolet Cross-Sections of Ozone: I. The Measurements", Proceedings of the Quadrennial Ozone Symposium, Halkidiki, Greece, D. Reidel publishing Co., Dordrecht, 606-610 (1984)

Bates, R.D.: "Rayleigh Scattering by Air", *Planet. Space Sci.* **32**, 785-790 (1984)

Bohren, C.F. and D.R. Huffman: "Absorption and Scattering of Light by Small Particles", Wiley, New York (1983)

Bojkov, R.D.: "Differences in Dobson Spectrophotometer and Filter Ozonometer Measurements of Total Ozone", *J. Appl. Meteorology* **8**, 362-368 (1969)

CEC: "Environmental UV Radiation - Causes - Effects - Consequences", J. Acevedo and C. Nolan (Eds.), CEC, DG XII, Brussels (1993)

Bucholtz, A.: " Rayleigh-Scattering Calculations for the Terrestrial Atmosphere", *Appl. Opt.* **34**, 2765-2773 (1995)

Crutzen, P.J. and P.H. Zimmermann: "The Changing Photochemistry of the Troposphere", *Tellus* **43AB**, 136-151 (1991)

De Haan, J.F., P.B. Bosma and J.W. Hovenier: "The Adding Method for Multiple Scattering Calculations of Polarized Light", *Astron. Astrophys.* **183**, 371-391 (1987)

Dobson, G.M.B.: "Observer's Handbook for the Ozone Spectrophotometer", *Ann. IGY* **5**, 46-114 (1957)

Farman, J.C., B.G. Gardiner and J.D. Shaklin: "Large Losses of Total Ozone in Antarctica Reveal Seasonal ClO_x/NO_x Interaction", *Nature* **315**, 207-210 (1985)

Fortuin, J.P.F., and H. Kelder: "Possible Links between Ozone and Temperature Trends" submitted to *Geophys. Res. Lett.* (1996)

Green, A.E.S., T. Sawada and E.P. Shettle: "The Middle Ultraviolet Reaching the Ground", *Photochem. Photobiol.* **19**, 251-259 (1974)

Green, A.E.S., K.R. Cross and L.A. Smith: "Improved Analytic Characterization of Ultraviolet Skylight", *Photochem. Photobiol.* **31**, 59-65 (1980)

Hansen, J.E. and L.D. Travis: "Light Scattering in Planetary Atmospheres", *Space Sci. Rev.* **16**, 527-610 (1974)

Hearn, C.H. and J.A. Joens: "The Near UV Absorption Spectrum of CS_2 and SO_2 at 300 K", *J. Quant. Spectrosc. Radiat. Transfer* **45**, 69-75 (1991)

IPCC: "Climate Change 1994", J.T. Houghton *et al.* (Eds.), Cambridge University Press, Cambridge (1995)

Iqbal, M.: "An Introduction to Solar Radiation", Academic Press, New York, NY (1983)

Josefsson, W.A.P.: "Focused Sun Observations Using a Brewer Ozone Spectrophotometer", *J. Geophys. Res.* **97** # D14, 15813-15817 (1992)

Kasten, F. and A.T. Young: "Revised Optical Air Mass Tables and Approximation Formula", *Appl. Opt.* **28**, 4735-4738 (1989)

Kerr, J.B., C.T. McElroy and R.A. Olafson: "Measurements of Ozone with the Brewer Spectrophotometer", Proc. Quadr. Ozone Symp. **1**, 74-79, Boulder, CO (1980)

Kinnison, D.E., K.E. Grant, P.S. Connell, D.A. Rotman and D.J. Wuebbles: "The Chemical and Radiative Effects of the Mount Pinatubo Eruption", *J. Geophys. Res.* **99**, # D12, 25705-25731 (1994)

Kneizys, F.X., E.P. Shettle, L.W. Abreu, J.H. Chetwind, G.P. Anderson, W.O. Gallery, J.E.A. Selby and S.A. Clough: "Users Guide to LOWTRAN 7", Air Force Geophysics Laboratory, AFGL-TR-88-0177, Environmental Research Papers No. 1010, Hanscom, MA (1988)

Kuik, F. and H. Kelder: "Spectral Ultraviolet Radiation Measurements and Correlation with Atmospheric Parameters", KNMI, Scientific Report WR 94-05, De Bilt (1994)

Leckner, B.: "The Spectral Distribution of Solar Radiation at the Earth's Surface - Elements of a Model", *Sol. Energy* **20**, 143-150 (1978)

Lenoble, J.: "Atmospheric Radiative Transfer", A. Deepak Publ., Hampton, VA (1993)

Matthews, W.A., R.E. Basher and G.J. Fraser: "Filter Ozone Spectrophotometer" *Pure Appl. Geophys.* **112** 931-938 (1974)

McClatchey, R.A., R.W. Fenn, J.E.A. Selby, F.E. Volz and J.S.Garing: " Optical Properties of the Atmosphere (Third Edition)", AFGL Environmental Research Papers No. 411, Hanscom, MA (1972)

Mims, F.M.: "How to Measure the Ozone Layer", *Scientific American* November,

45-51 (1992)

Paur, R.J. and A.M. Bass: "The Ultraviolet Cross-Sections of Ozone: II. Results and Temperature Dependence", Proceedings of the Quadrennial Ozone Symposium, Halkidiki, Greece, D. Reidel publishing Co., Dordrecht, 611-616 (1984)

Peck, E.R. and K. Reeder: "Dispersion of Air", *J. Opt. Soc. Am.* **62**, 958-962 (1972)

Radiation Commission of IAMAP: "A preliminary Cloudless Standard Atmosphere for Radiation Computation", WCP-112, WMO/TD No. 24 (1986)

Schneider, W., G.K. Moortgat, G.S. Tyndall and J.P. Burrows: "Absorption Cross Sections of NO_2 in the UV and Visible Region (200-700 nm) at 298 K", *J. Photochem. Photobiol.* **40A**, 195-217 (1987)

Spencer, J.W.: "Fourier Series Representation of the Position of the Sun", *Search* **2**, 172 (1971)

Stammes, P., D. Stam, W.M.F. Wauben and F. Kuik: "Simulation and Interpretation of Atmospheric UV-VIS Spectra using the DAK Radiative Transfer Model", Proceedings of the Third European Symposium on Polar Stratospheric Ozone Research, 18-22 September 1995, Schliersee, Germany, to appear in Air Pollution Research Report Series (1996)

WMO, "Report of the International Ozone Trends Panel 1988", Global Ozone Research and Monitoring Project, Report No. 18, World Meteorological Organization, Geneva (1988)

WMO, "Scientific Assessment of Ozone Depletion", Global Ozone Research and Monitoring Project, Report No. 37, World Meteorological Organization, Geneva (1994)

VanHoosier, M.E., J.D. Bartoe, G.E. Bruecker and D.K. Prinz: "Absolute Solar Spectral Irradiance 120 nm -400 nm", *Astro. Lett. and Communications* **27**, 163-168 (1988)

KNMI-Publicaties, Technische & Wetenschappelijke Rapporten gepubliceerd sedert 1988

Een overzicht van alle publicaties van het Koninklijk Nederlands Meteorologisch Instituut die tussen 1849 en 1987 werden uitgegeven, wordt u op verzoek toegezonden door de Bibliotheek van het KNMI, postbus 201, 3730 AE De Bilt, tel. 030 - 2 206 855, fax. 030 - 2 210 407.

	KNMI-publicatie met nummer:	
150-27	Normalen en extreme waarden van 15 hoofdstations voor het tijdvak 1961-90 / samenst. H.J. Krijnen ...[et al.]	1992
165-5	Historische weerkundige waarnemingen: beschrijving antieke meetreeksen / H.A.M. Geurts en A.F.V. van Engelen	1992
172	Vliegen in weer en wind: geschiedenis van de luchtvaartmeteorologie / Tj. Langerveld	1988
173	Werkdocument verspreidingsmodellen / red. H. van Dop ; in samenwerking met het RIVM	1988
174	Ons klimaat, onze planeet / voorw. H. Tennekes ; inleiding C.J.E. Schuurmans ; met bijdr. van H. van Dop ...[et al.]	1989
175	Klimaat-onderzoek Westland ten behoeve van kustuitbreiding / W.H. Slob	1989
176	Stormenkalender: chronologisch overzicht van alle stormen langs de Nederlandse kust 1964-1990 / B. Augustijn, H. Daan ...[et al.]	1990
177	Description of the RIVM-KNMI PUFF dispersion model / G.H.L. Verver ...[et al.]	1990
178	Modules A & B / Bureau Vorming en Opleiding **[uitsluitend intern beschikbaar]**	1991-
179	Catalogus van aardbevingen in Nederland / G. Hougast	1991
179a	Catalogus van aardbevingen in Nederland : 2e, gewijzigde druk / G. Houtgast	1992
180	List of acronyms in environmental sciences / [P. Geerders]	1991
180a	List of acronyms in environmental sciences : revised edition / [P. Geerders and M. Waterborg]	1995
181	Nationaal gebruik van de groepen 7wwW1W2 en 960ww voor landstations / [samenst. H. van Drongelen ea.]	1992
181a	FM12 Synop : internationale en nationale regelgeving voor het coderen van de groepen 7wwW1W2 en 960ww	1995
182	Wijziging aeronautische codes : 1 juli 1993 / [P.Y. de Vries en A.A. Brouwer]	1993
183-1	Rainfall in New Guinea (Irian Jaya) / T.B. Ridder	1995
183-2	Vergelijking van zware regens te Hollandia (Nieuw Guinea), thans Jayapura (Irian Jaya) met zware regens te De Bilt / T.B. Ridder	1995
183-3	Verdamping in Nieuw-Guinea, vergelijking van gemeten hoeveelheden met berekende hoeveelheden / T.B. Ridder	1995
183-4	Beschrijving van het klimaat te Merauke, Nieuw Guinea (Irian Jaya) in verband met de eventuele vestiging van een zoutwinningsbedrijf aldaar / T.B. Ridder en H.W.H. Weeda	1995
183-5	Overzicht van klimatologische en geofysische publikaties betreffende Nieuw-Guinea / T.B. Ridder	1995
184	Inleiding tot de algemene meteorologie : studie-uitgave / B. Zwart, A. Steenhuisen, m.m.v. H.J. Krijnen	1994
184a	Inleiding tot de algemene meteorologie : studie uitgave ; 2e, geheel herziene druk / B. Zwart, A. Steenhuisen, m.m.v. H.J. Krijnen ea.	1995
185	Handleiding voor het gebruik van sectie 2 van de FM 13-X SHIP code door stations op zee / KNMI; Kon. Luchtmacht; Kon. Marine	1994
185a	Handleiding voor het gebruik van sectie 2 van de FM 13-X SHIP-code voor waarnemers op zee / KNMI; Kon.Luchtmacht, Kon.Marine	1995
(-)	Zonnestraling in Nederland / C.A. Velds (i.s.m. uitgeverij Thieme in de serie Het klimaat van Nederland; 3)	1992

	Technisch rapport = technical report (TR) - ISSN 0169-1708	
103a	Wind-chill [geheel herziene versie] / B. Zwart	1992
105	Description of the Cabauw turbulence dataset 1977-1979 / C. Hofman	1988
106	Automatische detektie van inversies met sodar / A.C.M. Beljaars en R. Agterberg	1988
107	Numerieke atmosfeermodellen / A.P.M. Baede	1988
108	Inpassing van Meteosat informatie in de meteorologische besluitvorming / J. Roodenburg	1988
109	Opmeting van het aardmagneetveld in Nederland, herleid naar 1985 / J.H. Rietman	1988
111	Van Penman naar Makkink: een nieuwe berekeningswijze voor de klimatologische verdampingsgetallen / red. J.C. Hooghart ...[et al.]	1988
112	Description of a software library for the calculation of surface fluxes / A.C.M. Beljaars ...[et al.]	1989
113	Menghoogteberekeningen voor het Europees continent: een vergelijkend onderzoek / M.P. Scheele en H. van Dop	1989
114	Operational WAMS statistics over the period December 1986 - March 1987 / R.A. van Moerkerken ...[et al.]	1989
115	Mesoscale terrain roughness mapping of the Netherlands / R. Agterberg and J. Wieringa	1989
116	Geschiedenis van de landbouwmeteorologie in Nederland tot 1972 / J.P.M. Woudenberg	1989
117	Instabiliteiten rond de straalstroom / R.P. Henzen	1989
118	Verfificatie van de GONO golfverwachting over de periode oktober 1987 - april 1988 / R.A. van Moerkerken	1989
119	Spectra en gradienten van hoge windsnelheden te Cabauw tot 200 meter / R.W.M. Meijer	1989
120	About the possibilities of using an air transformation model in Tayun, Shanxi province, China / J. Reiff ...[et al.]	1989
121	The effect of wave data assimilation of the numerical simulation of wave energy advection / M. de las Heras ...[et al.]	1990
122	Objective analysis of precipitation observations during the Chernobyl episode / M.P. Scheele and G.H. Verver	1990
123	The use of satellite data in the ECMWF analysis system / K. Lablancz	1990
124	A primitive equation model for the Equatorial Pacific / M.A.F. Allaart and A. Kattenberg	1990
125	Technical description of the high-resolution air mass transformation model at KNMI / E.I.F. de Bruin ...[et al.]	1990
126	Verificatie kwantitatieve neerslagverwachting korte termijn (proefperiode) voor 5 regio's / D. Messerschmidt	1990
127	Quantitative processing of Meteosat-data: implementation at KNMI: applications / S.H. Muller	1990
128	A primary experiment of statistical interpolation schemes used in sea wave data assimilation / Gao Quanduo	1990
129	Coordinate conversions for presenting and compositing weather radar data / H.R.A. Wessels	1990
130	Flux-profile relationships in the nocturnal boundary layer / P. Bouwman	1990
131	The implementation of the WAQUA/CSM-16 model for real time storm surge forecasting / J.W. de Vries	1991
132	De luchttemperatuur boven West-Ameland / F. Ynsen	1991
133	Seizoenverloop en trend in de chemische samenstelling van de neerslag te Lelystad / T.A. Buishand en J.H. Baard	1991
134	Technical description of LAM and OI: Limited Area Model and Optimum Interpolation analysis / W.C. de Rooy ...[et al.]	1991
134a	Technical description of LAM and OI: Limited Area Model and Optimum Interpolation analysis, 2nd edition / W.C. de Rooy ...[et al.]	1992
135	Relatieve trajectorien in en rond een depressie / J.P.A.J. van Beeck	1991
136	Bepaling van een directe en diffuse straling en van zonneschijnduur uit 10-minuutwaarden van de globale straling / W.H. Slob ...[et al.]	1991
137	LAM en NEDWAM statistics over the period October 1990 - April 1991 / R.A. van Moerkerken	1991
138	Dagsom van de globale straling : een rekenmethode en verwachtingsverificatie / M.C. Nolet	1991
139	A real-time wave data quality control algorithm / Maria Paula Etala	1991
140	Syllabus Fysische Meteorologie I / H.R.A. Wessels	1991
141	Systeembeschrijving Mist Voorspel Systeem MIVOS / D. Blaauboer, H.R.A. Wessels en S. Kruizinga	1992
142	Het nachtelijk windmaximum : een interactieve verwachtingsmethode / N. Maat en H. Bakker	1992

143 Neerslagverificatie LAM / W.C. de Rooy en C. Engeldal 1992
144 Aanpassing vocht-bedekkingsgraadrelaties in het LAM / W.C. de Rooy 1992
145 Een verificatie van de Eurogids, de gidsverwachting voor vervoer en toerisme / H.G. Theihzen 1992
146 The earth radiation budget experiment : overview of data-processing and error sources / Arnout J. Feijt 1992
147 On the construction of a regional atmospheric climate model / Jens H. Christensen and Erik van Meijgaard 1992
148 Analyse van torenwindgegevens over het tijdvak 1977 tot en met 1991 / Gertie Geertsema 1992
149 The performance of drag relations in the WAQUA storm surge model / J.R.N. Onvlee 1993
150 Verifications of 3I retrievals vis-à-vis radiosonde observations / G.J. Prangsma 1993
151 Het Synoptisch Symposium : een verslag / red. H.G. Theihzen 1993
152 The ACIFORN hydrological programme : the water cycle of a Douglas fir forest / F.C. Bosveld ...[et al.] 1993
153 Het APL+-prgramma / R.M. van Westrhenen 1993
154 The effect of spatial averaing on threshold exceedances of daily precipitation amounts / T.A. Buishand, 1993
155 Neerslagvergelijking van Espelo ten opzichte van het omgevingsgemiddelde / J.P.M. van Dun en J. Verloop 1993
156 On the effects of limited spectral resolution in third-generation wave models / I.V. Lavrenov and J.R.A. Onvlee 1993
157 Meteorologische evaluatie van de zichtmetingen langs de A16 / H.R.A. Wessels 1993
158 Het programma voor berekening van zonneschijnduur uit globale straling / U. Bergman 1993
159 Verificatie weersverwachtingen 1955 - 1993 / H. Daan 1993
160 Drie objectieve indices voor clear-air turbulence nader bekeken / H. Bakker 1993
161 The ASGASEX experiment / W.A. Oost 1994
162 TEBEX observations of clouds and radiation -potential and limitations / P. Stammes ...[et al.] 1994
163 Evaluatie kwaliteitsonderzoek mistdata "Mistprojekt A-16" Breda / M. van Berchum 1994
164 Standaard stralingsmetingen met een zonnevolger / A.C.A.P. van Lammeren en A. Hulshof 1994
165 Neurale netwerken versus lineaire regressie / R.M. Meuleman 1994
166 Seismische analyse van de aardbeving bij Alkmaar op 6 augustus 1994 / [SO] 1994
167 Seismische analyse van de aardbeving bij Alkmaar op 21 september 1994 / [SO] 1994
168 Analyse van het seismische risico in Noord-Nederland / Th. de Crook, B. Dost en H.W. Haak 1995
169 Evaluatie van neerslagprognoses van numerieke modellen voor de Belgische Ardennen in december 1993 / Erik van Meijgaard 1994
170 DARR-94 / C.P.G. Lomme 1994
171 EFEDA-91 : documentation of measurements obtained by KNMI / W.A.A. Monna ...[et al.] 1994
172 Cloud lidar research at the Royal Netherlands Meteorological Institute and KNMI2B2 version 2 cloud lidar analysis software documentation / Alexandre Y. Fong and André C.A.P. van Lammeren 1994
173 Measurements of the structure parameter of vertical wind-velocity in the atmospheric boundary layer / R. van der Ploeg 1995
174 Report of the ASGASEX'94 workshop / ed. by W.A. Oost 1995
175 Over slecht zicht, bewolking, windstoten en gladheid / J. Terpstra 1995
176 Verification of the WAQUA/CSM-16 model for the winters 1992-93 and 1993-94 / J.W. de Vries 1995
177 Nauwkeuriger nettostraling meten / M.K. van der Molen en W. Kohsiek 1995
178 Neerslag in het stroomgebied van de Maas in januari 1995: waarnemingen en verificatie van modelprognoses / Rudmer Jilderda ...[et al.] 1995
179 First field experience with 600PA phased array sodar / Henk Klein Baltink 1995
180 Een Kalman-correctieschema voor de wegdektemperatuurverwachtingen van het VAISALA-model / A. Jacobs 1995
181 Calibration study of the K-Gill propeller vane / Marcel Bottema 1995
182 Ontwikkeling van een spectraal UV-meetinstrument / Frank Helderman 1995
183 Rainfall generator for the Rhine catchment : a feasibility study / T. Adri Buishand and Theo Brandsma 1996
184 Parametrisatie van mooi-weer cumulus / M.C. van Zanten 1995
185 Interim report on the KNMI contributions to the second phase of the AERO-project / Wiel Wauben, Paul Fortuin ...[et al.] 1995
186 Seismische analyse van de aardbevingen bij Middelstum (30 juli 1994) en Annen (16 augustus 1994 en 31 januari 1995) / [SO] 1995
187 Analyse wenselijkheid overname RIVM-windmeetlokaties door KNMI / H. Benschop 1996
188 Windsnelheidsmetingen op zeestations en kuststations: herleiding waarden windsnelheden naar 10-meter niveau / H. Benschop 1996
189 On the KNMI calibration of net radiometers / W. Kohsiek 1996
190 NEDWAM statistics over the period October 1994 - April 1995 / F.B. Koek 1996
191 Description and verification of the HIRLAM trajectory model / E.I.F. de Bruijn 1996
192 Tiltmeting : een alternatief voor waterpassing ? / H.W. Haak 1996

Wetenschappelijk rapport = scientific report (WR) - ISSN 0169-1651

88-01 Central Sudan surface wind data and climate characteristics / E.H. ABu Bakr
88-02 Startocumulus modeling / P.G. Duynkerke
88-03 Naar een niet-linear wateropzetmodel : stand van zaken februari 1988 / C.J. Kok
88-04 The boundary layer wind regime of a representative tropical African region, central Sudan / E.H. ABu Bakr
88-05 Radiative cooling in the nocturnal boundary layer / S.A. Tjemkes
88-06 Surface flux parameterization schemes : developments and experiences at KNMI / A.A.M. Holtslag and A.C.M. Beljaars
89-01 Instability mechanisms in a barotropic atmsophere / R.J. Haarsma
89-02 Climatological data for the North Sea based on observations by volutary observing ships over the period 1961-1980 / C.G. Korevaar
89-03 Verificatie van GONO golfverwachtingen en van Engelse fine-mesh winden over de periode oktober 1986 - april 1987 / R.A. van Moerkerken
89-04 Diagnostics derivation of boundary layer parameters from the outputs of atmospheric models / A.A.M. Holtslag ...[et al.]
89-05 Statistical forecasts of sushine duration / Li Zhihong and S. Kruizinga
90-01 The effect of a doubling atmospheric CO2 on the stormtracks in the climate of a GCM / P.C. Siegmund
90-02 Analysis of regional differences of forecasts with the multi-layer AMT-model in the Netherlands / E.I.F. de Bruin, Li Tao Guang ...[et al.]
90-03 Description of the CRAU- data-set: Meteosat data, radiosonde data, sea surface temperatures : comparison of Meteosat and Heimann-data / S.H. Muller, H. The, W. Kohsiek and W.A.A. Monna
90-04 A guide to the NEDWAM wave model / G. Burgers
91-01 A parametrization of the convective atmospheric boundary layer and its application into a global climate model / A.A.M. Holtslag ...[et al.]
91-02 Turbulent exchange coefficients over a Douglas fir forest / F.C. Bosveld
92-01 Experimental evaluation of an arrival time difference lightning positioning system / H.R.A. Wessels
92-02 GCM control run of UK Met.Office compared with the real climate in the Northwest European winter / J.J. Beersma
92-03 The parameterization of vertical turbulent mixing processes in a General Circulation Model of the Tropical Pacific / G. Janssen
92-04 A scintilation experiment over a forest / W. Kohsiek
92-05 Grondtemperaturen / P.C.T. van der Hoeven en W.N. Lablans
92-06 Automatic supression of anomalous propagation clutter for noncoherent weather radars / H.R.A. Wessels ...[et al.]

93-01 Searching for stationary stable solutions of Euler's equation / R. Salden
93-02 Modelling daily precipitation as a function of temperature for climatic change impact studies / A.M.G. Klein Tank and T.A. Buishand
93-03 An analytical conceptual model of extratropical cyclones / L.C. Heijboer
93-04 A synoptic climatology of convective weather in the Netherlands / Dong Hongnian
93-05 Conceptual models of severe convective weather in the Netherlands / Dong Hongnian
94-01 Seismische analyse van aardbevingen in Noord-Nederland : bijdrage aan het multidisciplinaire onderzoek naar de relatie tussen gaswinning en aardbevingen / H.W. Haak en Th. de Crook
94-02 Storm activity over the North Sea and the Netherlands in two climate models compared with observations / J.J. Beersma
94-03 Atmospheric effects of high-flying subsonic aircraft / W. Fransen
94-04 Cloud-radiation-hydrological interactions : measuring and modeling / A. Feijt ...[et al.]
94-05 Spectral ultraviolet radiation measurements and correlation with atmospheric parameters / F. Kuik and H. Kelder
95-01 Transformation of precipitation time series for climate change impact studies / A.M.G. Klein Tank and T.A. Buishand
95-02 Internal variability of the ocean generated by a stochastic forcing / M.H.B. van Noordenburg
95-03 Applicability of weakly nonlinear theory for the planetary-scale flow / E.A. Kartashova
95-04 Changes in tropospheric NOx and O3 due to subsonic aircraft emissions / W.M.F. Wauben ...[et al.]
95-05 Numerical studies on the Lorenz-84 atmosphere model / Leonardo Anastassiades
95-06 Regionalisation of meteorological parameters / W.C. de Rooy
95-07 Validation of the surface parametrization of HIRLAM using surface-based measurements and remote sensing data / A.F. Moene, H.A.R. de Bruin ...[et al.]
95-08 Probabilities of climatic change : a pilot study / Wieger Fransen (ed.) and Alice Reuvekamp
96-01 A new algorithm for total ozone retrieval from direct sun measurements with a filter instrument / W.M.F. Wauben